nature medicine

ARTICLES

https://doi.org/10.1038/s41591-018-0002-1

Stimulation of entorhinal cortex–dentate gyrus circuitry is antidepressive

Sanghee Yun[1,2], Ryan P. Reynolds[2], Iraklis Petrof[2], Alicia White[2], Phillip D. Rivera[3,5], Amir Segev[3], Adam D. Gibson[2], Maiko Suarez[2], Matthew J. DeSalle[2], Naoki Ito[3,6], Shibani Mukherjee[3], Devon R. Richardson[3], Catherine E. Kang[4], Rebecca C. Ahrens-Nicklas[2], Ivan Soler[1,2], Dane M. Chetkovich[4,7], Saïd Kourrich[3], Douglas A. Coulter[1,2] and Amelia J. Eisch[1,2,3*]

Major depressive disorder (MDD) is considered a 'circuitopathy', and brain stimulation therapies hold promise for ameliorating MDD symptoms, including hippocampal dysfunction. It is unknown whether stimulation of upstream hippocampal circuitry, such as the entorhinal cortex (Ent), is antidepressive, although Ent stimulation improves learning and memory in mice and humans. Here we show that molecular targeting (Ent-specific knockdown of a psychosocial stress-induced protein) and chemogenetic stimulation of Ent neurons induce antidepressive-like effects in mice. Mechanistically, we show that Ent-stimulation-induced antidepressive-like behavior relies on the generation of new hippocampal neurons. Thus, controlled stimulation of Ent hippocampal afferents is antidepressive via increased hippocampal neurogenesis. These findings emphasize the power and potential of Ent glutamatergic afferent stimulation—previously well-known for its ability to influence learning and memory—for MDD treatment.

Antidepressant medications are widely used to treat major depressive disorder (MDD), but 50% of patients with depression who receive these medications relapse, and 30% are drug-resistant[1,2]. MDD is marked by disordered activity of neuronal circuits that regulate mood, cognition, perception, reward, and motor function. However, both deep brain stimulation (DBS) and more superficial stimulation approaches (i.e., transcranial direct current stimulation (tDCS), transmagnetic stimulation (TMS), and electroconvulsive therapy (ECT)) have drawbacks, including cognitive side effects, seizures, and a high rate of relapse after remission[3]. Therefore, more treatments for MDD are needed, particularly stimulation therapies that more precisely target depression-linked dysfunctional circuitry.

Notable hallmarks of MDD are the structural and functional deficits apparent in the hippocampus, a brain region linked to mood regulation and memory. For example, depressed humans and chronically stressed animals have reduced hippocampal activity and volume and decreased expression of activity-dependent genes and processes, including reduced adult neurogenesis in the hippocampal dentate gyrus (DG)[4,5]. These hippocampal deficits have long been the target of depression treatments in an effort to ameliorate depression symptoms[5,6]. Interestingly, DBS of a major source of hippocampal inputs, the entorhinal cortex (Ent), enhances hippocampal-dependent memory in humans and mice and increases DG neurogenesis in rodents[7,8]. Although Ent volume is decreased in late-onset and remitted MDD[9], it is unknown whether specific stimulation of Ent–DG afferents combats the symptoms of depression.

Here we used molecular and chemogenetic approaches to test whether Ent–DG stimulation is antidepressive in mice. For the molecular approach, we targeted tetratricopeptide-repeat-containing RAB8b-interacting protein (TRIP8b, also called PEX5R), a brain-specific auxiliary subunit of the hyperpolarization-activated cyclic nucleotide–gated (HCN) channel[10]. TRIP8b splice variants differentially regulate cell surface expression of HCN channels and their hyperpolarization-activated current (I_h)[11–13]. Notably, disruption of TRIP8b (germline knockout) or HCN1 function (hippocampal-specific knockdown) increases the excitability of hippocampal neurons and results in antidepressive-like behavior[11,14]. Using viral-mediated knockdown of TRIP8b in Ent neurons, we found that disinhibited Ent afferents to the DG drive activity-dependent processes in the DG and facilitate antidepressive-like behavior under both basal and stressful conditions. Mechanistically, we found that this antidepressive-like behavior was dependent on adult hippocampal neurogenesis. As our viral-mediated TRIP8b knockdown targeted all neurons in the Ent, we next used viral-mediated gene transfer, transgenic mice, and chemogenetics[15] to determine whether stimulation specifically of glutamatergic Ent–DG circuitry drove antidepressive-like behavior. We found that chronic stimulation of glutamatergic afferents from the Ent to the DG ameliorates behavioral symptoms of depression under both acute and chronic stressful conditions.

Results

***Trip8b* germline knockout mice have increased dentate gyrus neurogenesis and dendritic morphology relative to wild-type mice.** Hippocampal neurons fire more frequently in *Trip8b* germline knockout mice owing to lack of I_h[11], and *Trip8b* germline knockout mice display antidepressive-like behavior[11]. Given the links among antidepressive-like behavior, hippocampal activity, and DG neurogenesis[5], we hypothesized that *Trip8b* germline knockout

[1]Perelman School of Medicine, University of Pennsylvania, Philadelphia, PA, USA. [2]Children's Hospital of Philadelphia Research Institute, Philadelphia, PA, USA. [3]Department of Psychiatry, University of Texas Southwestern Medical Center, Dallas, TX, USA. [4]Department of Neurology and Clinical Neurological Sciences, Northwestern University, Chicago, IL, USA. [5]Present address: Department of Pediatrics, Massachusetts General Hospital for Children, Charlestown, MA, USA. [6]Present address: Oriental Medicine Research Center, Kitasato University, Tokyo, Japan. [7]Present address: Department of Neurology, Vanderbilt University Medical Center, Nashville, TN, USA. *e-mail: eischa@email.chop.edu

mice would have more DG neurogenesis. Indeed, 8-week-old male and female *Trip8b* germline knockout mice had more DG neurogenesis than control littermates (Supplementary Fig. 1), particularly in the temporal DG, a subregion related to stress response and emotion[16,17].

Psychosocial stress increases the level of a specific TRIP8b isoform in the dentate gyrus. Epifluorescent immunohistochemical analysis in 8-week-old wild-type C57BL/6J mice revealed TRIP8b protein in Ent layer II/III cell bodies and in their terminals in the molecular layer of the DG, but TRIP8b-immunoreactive (TRIP8b$^+$) cells and fibers in the granule cell layer of the DG were extremely sparse (Supplementary Fig. 2). This suggests that TRIP8b in Ent–DG projections—but not in DG-intrinsic cell bodies or their fibers—is poised to play a role in the activity-dependent processes of the hippocampus. To test this, we first considered that stress precipitates MDD in humans and depression-like symptoms in mice and rats[5,6]. The antidepressive-like behavior and increased neurogenesis in *Trip8b*-knockout mice and the presence of TRIP8b in the Ent–DG pathway led us to hypothesize that stress would increase TRIP8b levels in Ent–DG projections. Using a well-established chronic social defeat stress (CSDS) model of depression[18], we identified populations of mice that were either susceptible or resilient to a social stress: a 10-d defeat paradigm (Fig. 1a and Supplementary Fig. 3). Then, in stressed versus control mice, the Ent–DG circuit was analyzed for levels of the most predominant alternatively spliced isoforms of TRIP8b[12,13]: IsoA4 (containing exon 1a and exon 4), which upregulates surface expression of HCN channels and enhances I_h amplitude; IsoA5 (containing exon 1a but not exon 2 or exon 4), which reduces I_h; and IsoB (containing exon 1b and exon 2), which also abolishes I_h. Western blot analysis revealed 27% more TRIP8b isoform IsoA4 in the Ent–DG circuit of stressed (both susceptible and resilient) versus control mice (Fig. 1b,c), with no change in total TRIP8b, IsoA5, or IsoB levels (Fig. 1b,d,e and Supplementary Fig. 3i,l,o). Also, in resilient—but not susceptible—mice, the IsoA4 level was negatively correlated with social interaction ratio (SI ratio; Supplementary Fig. 3k). As IsoA4 maintains HCN channel surface expression and enhances I_h amplitude[12,13], higher levels of IsoA4 may be related to our hypothesis that there is decreased Ent–DG circuit activity after stress.

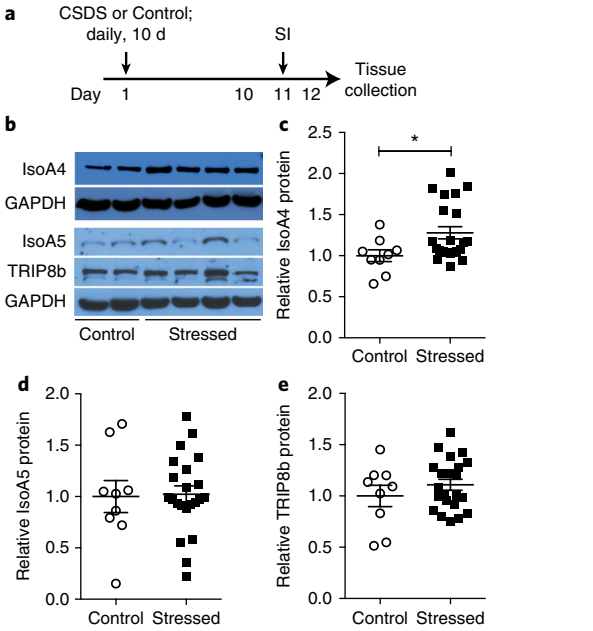

Fig. 1 | CSDS increases levels of TRIP8b isoform IsoA4 in the DG. **a**, The timeline for CSDS or control and SI experiments. **b**, Western blot of TRIP8b and major hippocampal TRIP8b isoforms, IsoA4 and IsoA5, in the DG of control and stressed mice. Levels are normalized to that of GAPDH. Uncropped blots are provided in Supplementary Fig. 3a–e. **c**–**e**, The level of IsoA4 (**c**), IsoA5 (**d**) and TRIP8b (**e**) in stressed and control mice. Levels are normalized to that of GAPDH. $n = 9$ control and 22 stressed mice. Statistical analysis was performed using an unpaired *t*-test: in **c**, $^*P < 0.05$; in **d** and **e**, $P > 0.05$. Data are shown as mean ± s.e.m. with data points from individual mice in **c**–**e**. See Supplementary Table 1 for detailed statistical information.

Entorhinal cortex–specific TRIP8b knockdown increases intrinsic excitability of stellate cells and enhances neurogenesis, but does not induce abnormal brain network activity. Considering that *Trip8b* germline knockout mice show antidepressive-like behaviors, that TRIP8b is expressed in the Ent–DG circuit, and that the major TRIP8b isoform, IsoA4, is increased in Ent–DG circuitry after stress, we next hypothesized that loss of TRIP8b specifically in Ent projections to the DG enhances activity-dependent processes in the DG and antidepressive-like behavior. We generated a virus to knock down TRIP8b (adeno-associated virus (AAV) encoding EGFP and shRNA targeting TRIP8b, referred to as 'TRIP8b shRNA'; Fig. 2a) and a control virus (AAV encoding EGFP and scrambled shRNA, referred to as 'SCR shRNA')[13] and used viral-mediated gene transfer to verify TRIP8b-knockdown efficiency in vitro (Fig. 2b,c and Supplementary Fig. 4a,b) and in vivo (Fig. 2d,e). In vitro, there was 87% less TRIP8b protein expression in TRIP8b-shRNA-transfected cells than in SCR-shRNA-transfected cells (Fig. 2b,c). In vivo, EGFP$^+$ cells in the Ent of TRIP8b-shRNA-infused mice rarely expressed TRIP8b (Fig. 2d,e), and when they did express TRIP8b, it was at a very low level. This suggested the ability of the shRNA to knock down levels of TRIP8b in vivo. To assess the functional impact of the virus in vivo, whole-cell current-clamp recordings were performed in brain slices 3–5 weeks after stereotaxic infusion of TRIP8b shRNA or SCR shRNA into the Ent of 7-week-old male C57BL/6J mice (Fig. 2f–h)[19]. Action potentials were more frequent in TRIP8b-shRNA-transfected EGFP$^+$ stellate cells than in SCR-shRNA-transfected EGFP$^+$ stellate cells and neighboring EGFP$^-$ stellate cells in both TRIP8b-shRNA-infused and SCR-shRNA-infused mice (Fig. 2g,h and Supplementary Fig. 4c–e), resulting in overall increased neuronal excitability. As brain stimulation approaches can have drawbacks, such as seizure induction or abnormal brain activity, in vivo electroencephalogram (EEG) recordings were performed in awake and behaving male and female mice 5 weeks after viral infusion in the Ent (Fig. 2i). In vivo EEG recordings revealed no abnormal or epileptiform activity in the cortex or the hippocampus, as power spectral density analysis showed similar brain activity in SCR-shRNA- and TRIP8b-shRNA-infused mice (Fig. 2i,j and Supplementary Fig. 4f,g). Neither SCR-shRNA- nor TRIP8b-shRNA-infused mice showed the epileptiform-like activity in the cortical–hippocampal network that was seen in pilocarpine-treated mice (Fig. 2j).

Having established in vitro and in vivo efficacy and the lack of abnormal activity in the cortical–hippocampal network, we next assessed the ability of Ent-specific knockdown of TRIP8b to promote an activity-dependent process in the DG, such as DG neurogenesis. Four weeks after viral infusion in the Ent, EGFP$^+$ DG molecular layer terminals were evident (Fig. 2k–m and Supplementary Fig. 5a–h). Ent-specific TRIP8b knockdown enhanced several indices of DG neurogenesis and new neuron maturation (Fig. 2n–w), as there were 11% more doublecortin (DCX)$^+$ cells (Fig. 2n,o), 55% more surviving BrdU$^+$ cells (Fig. 2p–q), and 64% more BrdU$^+$NeuN$^+$ neurons (Fig. 2r,s) in the DG of TRIP8b-shRNA-infused mice versus SCR-shRNA-infused mice, but there was no change in the number of type-1 neural stem cells (Supplementary Fig. 6). Dendritic reconstruction of DCX$^+$ cells showed dendrites that were 23% longer and

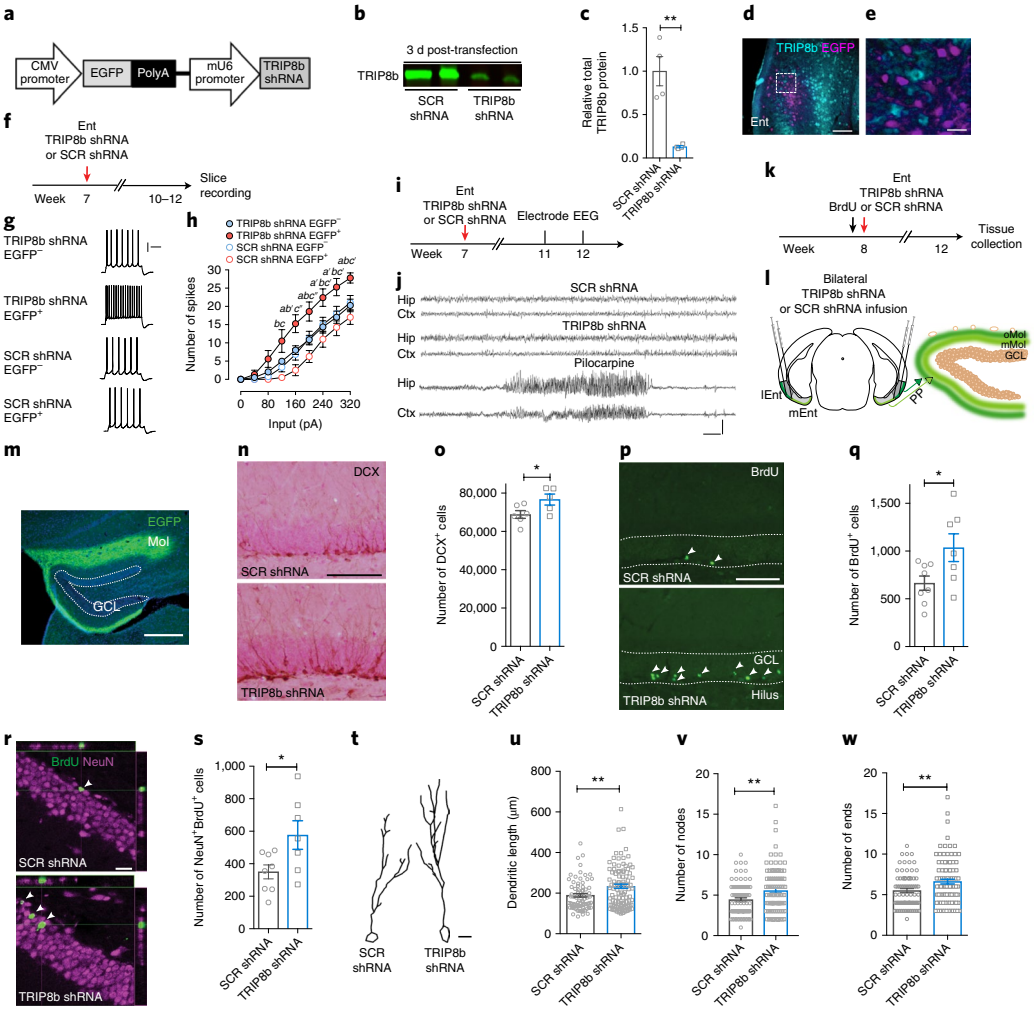

Fig. 2 | Ent-specific TRIP8b knockdown increases intrinsic excitability of Ent stellate cells and enhances DG neurogenesis. a, Schematic of the TRIP8b-targeted shRNA construct packaged into an AAV. **b**,**c**, Qualitative (**b**) and quantitative (**c**) in vitro efficacy of TRIP8b knockdown assessed via western blot. $n = 4$ SCR-shRNA-transfected wells, $n = 4$ TRIP8b-shRNA-transfected wells. Data in **c** are normalized to total protein staining level and presented as TRIP8b protein level relative to values from SCR-shRNA-transfected wells. Statistical analysis was performed using an unpaired *t*-test in **c**: $^{**}P < 0.01$. Uncropped blots are provided in Supplementary Fig. 4a,b. **d**,**e**, Photomicrographs of the Ent after immunohistochemistry staining for TRIP8b (teal) and EGFP (purple). No purple Ent cell bodies stained teal, supporting the in vivo efficiency of Ent-targeted TRIP8b knockdown, which is consistent with expression of EGFP$^+$ terminals in the molecular layer of the DG. The dashed box in **d** is magnified in **e**. Scale bars: **d**, 200 μm; **e**, 40 μm. **f**, The timeline of electrophysiology whole-cell patch experiments. **g**,**h**. Qualitative (**g**) and quantitative (**h**) ex vivo electrophysiological assessment of Ent stellate cells transfected in vivo shows EGFP$^+$ cells from TRIP8b-shRNA-infused mice ($n = 5$ cells, 3 mice) have more spikes than EGFP$^+$ cells from SCR-shRNA-infused mice ($n = 4$ cells, 4 mice) and EGFP$^-$ stellate cells from either TRIP8b-shRNA-infused mice ($n = 14$ cells, 4 mice) or SCR-shRNA-infused mice ($n = 13$ cells, 5 mice). Statistical analysis was performed using a two-way repeated-measures ANOVA in **h**: main effects of input, $F_{8,256} = 188.0$, $P < 0.0001$; treatment, $F_{3,32} = 4.143$, $P < 0.05$; subject, matching, $F_{32,256} = 13.87$, $P < 0.0001$; and input × treatment interaction, $F_{24,256} = 2.326$, $P < 0.001$. Bonferroni post hoc analysis was performed: TRIP8b shRNA EGFP$^+$ versus TRIP8b shRNA EGFP$^-$: *a*, $P < 0.05$; *a′*, $P < 0.01$; TRIP8b shRNA EGFP$^+$ versus SCR shRNA EGFP$^-$: *b*, $P < 0.05$; *b′*, $P < 0.01$; TRIP8b shRNA EGFP$^+$ versus SCR shRNA EGFP$^+$: *c*, $P < 0.05$; *c′*, $P < 0.01$; *c″*, $P < 0.001$. In **g**, calibration = 200 ms, 20 mV. **i**, Timeline of in vivo EEG, including surgical implantation of electrode and subsequent EEG recording. **j**, Qualitative assessment of hippocampal (Hip) and cortical (Ctx) EEG in awake and behaving mice revealed normal brain activity and no epileptiform activity after Ent infusion of either SCR shRNA or TRIP8b shRNA. Epileptiform activity was seen in positive control mice that received pilocarpine ~1 month prior to EEG. In **j**, calibration = 10 s, 0.5 mV. **k**, The timeline of neurogenesis studies. **l**, A schematic of viral stereotaxic infusion into the lateral and medial Ent (lEnt and mEnt, respectively) (left) and terminal expression in the outer and middle molecular layers (oMol and mMol, respectively) of the DG following viral infusion (right). **m**, EGFP$^+$ immunoreactivity in perforant path (pp) terminals in the oMol and mMol of the DG following stereotaxic infusion. The dotted lines in **m** delineate the DG granule cell layer (GCL). Scale bar, 200 μm. **n**–**s**, Qualitative (**n**,**p**,**r**) and quantitative (**o**,**q**,**s**) assessment showing an increase in the number of DCX$^+$ cells (**n**,**o**; $n = 6$ SCR-shRNA-infused mice, 5 TRIP8b-shRNA-infused mice), surviving BrdU$^+$ cells (**p**,**q**; $n = 8$ SCR-shRNA-infused mice, 7 TRIP8b-shRNA-infused mice) and BrdU$^+$NeuN$^+$ neurons (**r**,**s**; $n = 8$ SCR-shRNA-infused mice, 7 TRIP8b-shRNA-infused mice) in mice following TRIP8b shRNA infusion in the Ent relative to mice that received SCR shRNA infusion. An unpaired *t*-test was used for statistical analysis in **o**, **q**, and **s**: $^{*}P < 0.05$. The arrowheads in **p** and **r** mark cells expressing the relevant marker; the dotted lines in **p** delineate the DG GCL. Scale bars: **n** and **p**, 200 μm; **r**, 20 μm. **t**, Reconstruction of the dendritic tree of DCX$^+$ DG neurons in SCR-shRNA-infused mice versus TRIP8b-shRNA-infused mice. Scale bar, 10 μm. **u**–**w**, TRIP8b-shRNA-infused mice had longer DCX$^+$ dendrites (**u**) and more nodes (**v**) and ends (**w**) than SCR-shRNA-infused mice ($n = 76$ neurons in SCR-shRNA-infused mice, 95 neurons in TRIP8b-shRNA-infused mice, 4 or 5 mice per group). Statistical analysis was performed using an unpaired *t*-test in **u**–**w**: $^{**}P < 0.01$. Data are shown as mean ± s.e.m. in **c**, **h**, **o**, **q**, **s**, and **u**–**w** with data points from individual mice in **o**, **q**, and **s** or from cells **c** and **u**–**w**. See Supplementary Table 1 for detailed statistical information.

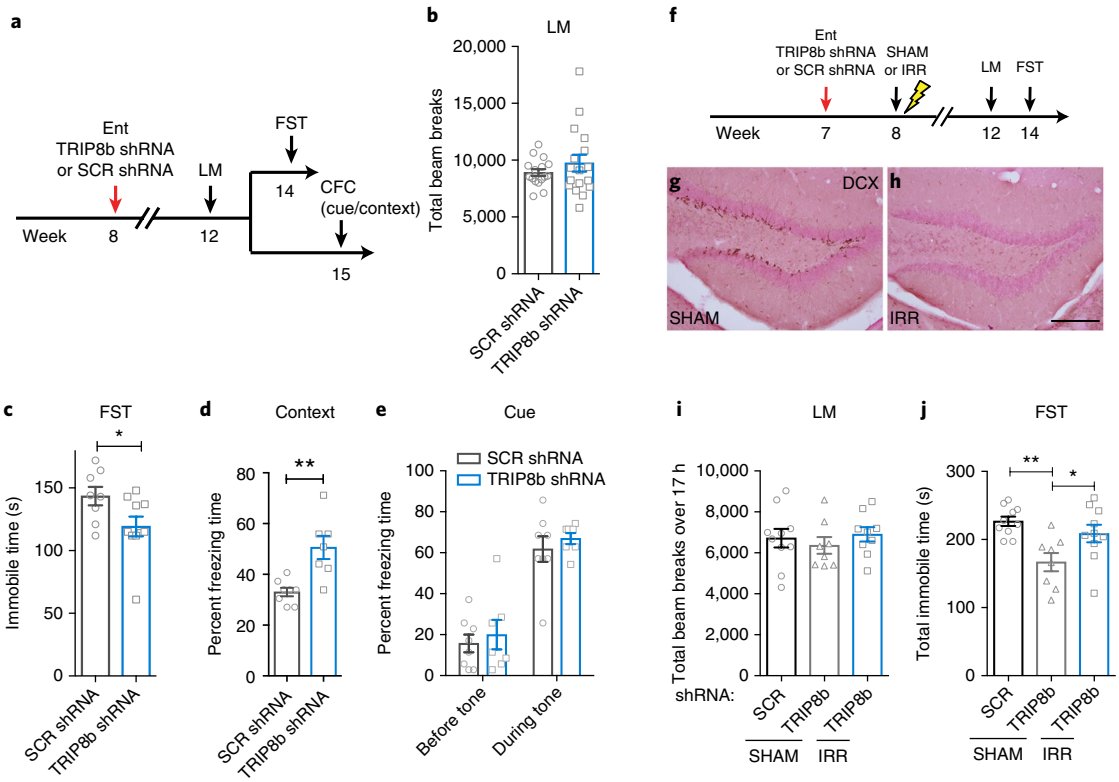

Fig. 3 | TRIP8b knockdown in the Ent induces antidepressive-like behavior that is neurogenesis-dependent. a, The timeline of viral infusion and behavioral testing. Four weeks following bilateral Ent infusion, mice were tested for locomotion (LM) and then were subjected to the forced swim test (FST) or contextual fear conditioning (CFC, consisting of training followed by context testing and then cue testing). **b**–**e**, TRIP8b shRNA infusion in the Ent did not change locomotion, as indicated by the number of beam breaks (**b**; $n = 16$ SCR-shRNA-infused mice, 17 TRIP8b-shRNA-infused mice), but decreased the time spent immobile in the forced swim test (**c**; $n = 8$ SCR-shRNA-infused mice, 10 TRIP8b-shRNA-infused mice) and increased time spent freezing in the contextual fear conditioning (**d**; $n = 8$ SCR-shRNA-infused mice, 7 TRIP8b-shRNA-infused mice) without altering time spent freezing in response to a cue following contextual fear conditioning (**e**; $n = 8$ SCR- shRNA-infused mice, 7 TRIP8b-shRNA-infused mice). Statistical analysis was performed using an unpaired *t*-test: in **b**, $P > 0.05$; in **c** and **d**, $^*P < 0.05$, $^{**}P < 0.01$. A two-way repeated-measures ANOVA was used in **e**: main effect of tone, $F_{1,13} = 55.16$, $P < 0.0001$; treatment, $F_{1,13} = 1.117$, $P > 0.05$; subjects, matching, $F_{13,13} = 0.5089$, $P > 0.05$; tone × treatment interaction, $F_{1,13} = 0.004857$, $P > 0.05$. **f**, The timeline of the neurogenesis ablation study. One week following bilateral Ent infusion, mice received sham irradiation (SHAM) or image-guided DG-targeted X-ray irradiation (IRR) to ablate DG neurogenesis. **g**,**h**, Photomicrographs from sham-treated (**g**) and IRR-treated (**h**) mice at 6 weeks following treatments showing depletion of DCX^+ cells in IRR-treated mice. Scale bar, 200 µm. **i**, Sham and IRR treatment groups did not differ in locomotion ($n = 10$ SCR shRNA/SHAM mice, 8 TRIP8b shRNA/SHAM mice, 9 TRIP8b shRNA/IRR mice). **j**, TRIP8b shRNA infusion in the Ent decreased the time spent immobile in the forced swim test relative to SCR-shRNA-infused, sham-treated mice. However, TRIP8b-shRNA-infused, IRR-treated mice spent more time immobile in the forced swim test than the TRIP8b-shRNA-infused, sham-treated mice ($n = 10$ SCR shRNA/SHAM mice, 8 TRIP8b shRNA/SHAM mice, 10 TRIP8b shRNA/IRR mice). Statistical analysis was performed using a one-way ANOVA in **i**: $F_{2,24} = 0.4149$, $P > 0.05$. A one-way ANOVA was used in **j**: $F_{2,25} = 7.07$, $P < 0.01$. Bonferroni post hoc analysis was performed: $^*P < 0.05$, $^{**}P < 0.01$. Data are shown as mean ± s.e.m. with data points from individual mice in **b**–**e**, **i**, and **j**. See Supplementary Table 1 and the Life Sciences Reporting Summary for detailed statistical information.

had 25% more nodes and 20% more ends (Fig. 2t–w)[20,21] in TRIP8b-shRNA-infused mice versus SCR-shRNA-infused mice. Thus, TRIP8b knockdown in Ent–DG afferents enhanced both the generation and dendritic maturation of adult-generated DG neurons.

Entorhinal cortex–specific TRIP8b knockdown promotes antidepressive-like behavior that is neurogenesis-dependent. As TRIP8b knockdown in the Ent–DG circuit enhanced DG neurogenesis—an activity-dependent process—and *Trip8b* germline knockout mice exhibited antidepressive-like behavior, we next hypothesized that Ent-specific TRIP8b knockdown would promote antidepressive-like behavior. Eight-week-old male mice received bilateral infusion of TRIP8b shRNA or SCR shRNA in the Ent. Four weeks later, these mice were tested for locomotor behavior and then examined in the forced swim test or for contextual fear conditioning (Fig. 3a). Compared to SCR-shRNA-infused mice, TRIP8b-shRNA-infused mice showed normal locomotor activity (Fig. 3b) but displayed antidepressive-like behavior, spending 17% less time immobile in the forced swim test (Fig. 3c). As the Ent–DG circuit is also involved in context-dependent memory[7], we hypothesized that Ent-specific TRIP8b knockdown would promote hippocampal-dependent memory after contextual fear conditioning. Indeed, TRIP8b-shRNA-infused mice displayed 51% more freezing in the shock-paired context versus SCR-shRNA-infused mice (Fig. 3d), with no difference in results from the cue test (Fig. 3e). Thus, Ent-specific TRIP8b knockdown indeed improved hippocampal-dependent memory.

Multiple lines of evidence implicate DG adult neurogenesis in antidepressant efficacy, particularly under stressful conditions[22–25]. Thus, the Ent-specific TRIP8b-knockdown-induced increase in neurogenesis may have been a causative factor in driving antidepressive-like behavior. However, it is also possible that the Ent-specific TRIP8b-knockdown-induced increase in neurogenesis observed here was merely correlated with the Ent-specific

TRIP8b-knockdown-induced antidepressive-like behavior, particularly after stress. To distinguish between these two possibilities, 7-week-old male mice received Ent infusion of TRIP8b shRNA or SCR shRNA, which was followed 1 week later by sham irradiation or DG-directed image-guided X-ray irradiation to ablate neurogenesis (Fig. 3f). Four weeks after irradiation, mice were assessed for locomotor activity and were subjected to the forced swim test after a brief restraint stress (Fig. 3f–j). As expected, ablation of neurogenesis did not change locomotor activity (Fig. 3i and Supplementary Fig. 7a). However, TRIP8b-shRNA-infused mice spent less time immobile in the forced swim test than the SCR-shRNA-infused mice, whereas DG-directed irradiation significantly blunted the antidepressive-like behavior inducedby Ent-specific TRIP8b knockdown (Fig. 3j and Supplementary Fig. 7b).

Entorhinal cortex–specific TRIP8b knockdown promotes antidepressive-like behaviors under conditions that mimic chronic stress. As TRIP8b knockdown in the Ent–DG circuit enhances antidepressive-like behavior under basal conditions and after a brief stress (Fig. 3c,j), we next hypothesized that TRIP8b knockdown in the Ent–DG circuit would enhance antidepressive-like behavior under conditions that mimic chronic stress, such as long-term exposure to the stress hormone corticosterone[26–29]. To test this hypothesis, 7-week-old female mice received Ent infusion of TRIP8b shRNA or SCR shRNA, and one week later, they began to receive chronic administration of corticosterone or vehicle (0.45% 2-hydroxypropyl-β-cyclodextrin; Fig. 4a). Behavioral testing for locomotion and anxiety- and antidepressive-like behavior—assessed through novelty-suppressed feeding as well as the forced swim test—began 4 weeks after viral infusion and 3 weeks into chronic corticosterone administration (Fig. 4b–g and Supplementary Figs. 8 and 9). Neither chronic corticosterone administration nor Ent-specific TRIP8b knockdown changed locomotor activity (Fig. 4b) or basal anxiety-like behavior in the dark–light test or in the elevated plus maze (Fig. 4c,d and Supplementary Fig. 9a–d). However, latency to feed in the novelty-suppressed feeding test was increased in mice that were chronically administered corticosterone relative to mice treated with vehicle (Supplementary Fig. 8a), and Ent-specific TRIP8b knockdown blocked this corticosterone effect (Fig. 4e and Supplementary Fig. 8a). Ent-specific TRIP8b knockdown did not change the corticosterone-induced effect on food consumption in mice in the home cage following novelty-suppressed feeding (Fig. 4f). Similarly, chronic corticosterone increased the time spent immobile in the forced swim test relative to mice treated with vehicle, whereas Ent-specific TRIP8b knockdown blocked this effect (Fig. 4g and Supplementary Fig. 8b).

One interpretation of these data is that Ent-specific TRIP8b knockdown promotes antidepressive-like behaviors under conditions that mimic chronic stress, but it is also possible that these effects are due to the action of Ent projections to other brain and hippocampal regions. However, analysis of behavioral data from mice that had additional 'off-target' expression (for example, terminal expression in hippocampal CA1 or CA2/CA3) revealed no antidepressive-like behavior in the forced swim test at baseline or after acute or chronic stress (Supplementary Fig. 5i–k). Thus, these data support the interpretation that TRIP8b knockdown in the Ent–DG circuit—and not in other brain or hippocampal areas—promotes antidepressive-like behavior.

Chronic stimulation of entorhinal cortex glutamatergic afferents drives dentate gyrus activity-dependent processes, but not abnormal network activity. Disinhibition of the Ent–DG circuit through TRIP8b knockdown promotes antidepressive-like behavior, suggesting that our manipulation was ultimately stimulating Ent excitatory neurons. To test whether stimulation of glutamatergic[30]—and not nonglutamatergic[31]—projections from the Ent

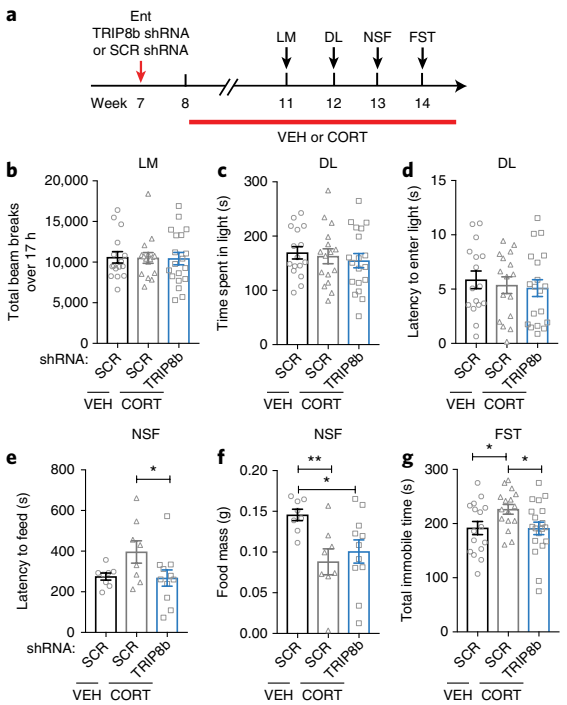

Fig. 4 | Ent-specific TRIP8b knockdown promotes antidepressive-like behaviors under conditions that mimic chronic stress. a, The timeline of viral infusion and behavioral testing. VEH, vehicle (2-hydroxypropyl-β-cyclodextrin); CORT, corticosterone; DL, dark–light test; NSF, novelty-suppressed feeding test. **b**, Corticosterone treatment did not change locomotion in either Ent SCR-shRNA- or TRIP8b-shRNA-infused mice relative to SCR-shRNA-infused, vehicle-treated mice ($n=16$ SCR shRNA/VEH mice, 16 SCR shRNA/CORT mice, 19 TRIP8b shRNA/CORT mice). Statistical analysis was performed using a one-way ANOVA in **b**: $F_{2,48}=0.01135$, $P>0.05$. **c**,**d**, In the dark–light test, corticosterone treatment did not change the time spent in light (**c**; $n=16$ SCR shRNA/VEH mice, 16 SCR shRNA/CORT mice, 19 TRIP8b shRNA/CORT mice) or the latency to enter light (**d**; $n=16$ SCR shRNA/VEH mice, 16 SCR shRNA/CORT mice, 19 TRIP8b shRNA/CORT mice) in either Ent SCR-shRNA- or TRIP8b-shRNA-infused mice relative to SCR-shRNA-infused, vehicle-treated mice. Statistical analysis was performed using a one-way ANOVA in **c**: $F_{2,48}=0.3328$, $P>0.05$. A one-way ANOVA was used in **d**: $F_{2,48}=0.249$, $P>0.05$. **e**,**f**, Corticosterone treatment reduced the latency to feed in the novelty-suppressed feeding test in TRIP8b-shRNA-infused mice relative to SCR-shRNA-infused, corticosterone-treated mice (**e**; $n=8$ SCR shRNA/VEH mice, 8 SCR shRNA/CORT mice, 11 TRIP8b shRNA/CORT mice). Food consumption in the home cage for both SCR-shRNA- and TRIP8b-shRNA-infused corticosterone-treated mice was significantly less than that of SCR-shRNA-infused vehicle-treated mice (**f**; food mass after the novelty-suppressed feeding test; $n=8$ SCR shRNA/VEH mice, 8 SCR shRNA/CORT mice, 11 TRIP8b shRNA/CORT mice). Statistical analysis was performed using a one-way ANOVA in **e**: $F_{2,24}=2.934$, $P=0.0725$. Fisher's LSD post hoc analysis was performed: $^{*}P<0.05$. A one-way ANOVA was used in **f**: $F_{2,24}=4.569$, $P<0.05$. Fisher's LSD post hoc analysis was performed: $^{*}P<0.05$, $^{**}P<0.01$. **g**, Corticosterone treatment led to more time immobile in the forced swim test in SCR-shRNA-infused mice than in SCR-shRNA-infused, vehicle-treated mice. However, TRIP8b-shRNA-infused, corticosterone-treated mice spent less time immobile in the forced swim test than SCR-shRNA-infused, corticosterone-treated mice ($n=16$ SCR shRNA/SHAM mice, 16 SCR shRNA/CORT mice, 19 TRIP8b shRNA/CORT mice). Statistical analysis was performed using a one-way ANOVA in **g**: $F_{2,48}=3.196$, $P<0.05$. Fisher's LSD post hoc analysis was performed: $^{*}P<0.05$. Data are shown as mean ± s.e.m. with data points from individual mice in **b**–**g**. See Supplementary Table 1 and the Life Sciences Reporting Summary for detailed statistical information.

to the DG are responsible for the observed effects, we used a chemogenetic approach[15] to control excitability of glutamatergic neurons in the Ent. Seven-week-old male and female mice expressing Cre recombinase under control of a CamKIIα promoter (CamKIIα-iCre mice[32]) received Ent infusion of a Cre-recombinase-dependent virus containing either the construct for the designer Gq-coupled modified human M3 muscarinic receptor (AAV-hSyn-DIO-hM3Dq-mCherry; referred to as 'hM3Dq') or a reporter construct (AAV-hSyn-DIO-mCherry; referred to as 'mCherry')[33] (Fig. 5a). Supporting appropriate targeting of the Ent–DG circuit (Fig. 5b,c and Supplementary Fig. 10a–h), CamKIIα-iCre-driven mCherry expression was evident in Ent cell bodies and DG molecular layer terminals of both hM3Dq-infused and mCherry-infused mice (Fig. 5c). After 4 weeks of daily administration of the designer ligand clozapine-*N*-oxide (CNO, intraperitoneal (i.p.)), c-Fos$^+$ cells were more abundant (suggesting more neural activity) in the Ent and DG of hM3Dq-infused mice relative to mCherry-infused mice (Fig. 5d,e and Supplementary Fig. 10i,j). The increase in c-Fos$^+$ cell number was hippocampal-subregion-specific, as there were 56% more c-Fos$^+$ cells in the DG of hM3Dq-infused mice than in mCherry-infused mice, but there was no difference in the number of c-Fos$^+$ cells in the CA1 and CA2/CA3 of hM3Dq-infused mice versus mCherry-infused mice (Fig. 5e). Stimulation of the Ent–DG circuit also increased DG neurogenesis, with 65% more BrdU$^+$ cells and 129% more BrdU$^+$NeuN$^+$ neurons in hM3Dq-infused mice than in mCherry-infused mice (Fig. 5f–j).

As stimulation of Ent–DG glutamatergic afferents might produce abnormal or epileptiform brain activity[34], we recorded cortical and hippocampal EEG of male and female CamKIIα-iCre mice that received hM3Dq or mCherry viral infusion into the Ent at 7 weeks of age and received CNO (1 mg per kg body weight (mg/kg), daily i.p., 5 weeks; Supplementary Fig. 11a) beginning 3 weeks later. In vivo EEG recordings of these awake and behaving mice revealed no aberrant epileptiform or hippocampal network activity after 5 weeks of CNO (1 mg/kg; Supplementary Fig. 11a–c,e–g) and no measurable difference in hippocampal network activity between hM3Dq mice and mCherry mice, even across the day–night cycle (Supplementary Fig. 11e–g). However, CNO-treated hM3Dq-infused mice given a single high dose of CNO (10 mg/kg) showed epileptiform activity (Supplementary Fig. 11d). These data reveal that hM3Dq-infused mice and mCherry-infused mice had similar hippocampal activity and support our ability to finely tune the activity of the Ent–DG circuit depending on the CNO dose.

Chronic stimulation of glutamatergic entorhinal cortical afferents to the dentate gyrus ameliorates behavioral symptoms of stress-induced depression. Having established that stimulation of the glutamatergic Ent–DG circuit enhances DG cellular activity and activity-dependent processes without driving abnormal brain network activity, we examined whether chronic chemogenetic stimulation of glutamatergic cells in the Ent drove antidepressive-like behaviors[24,35]. Seven-week-old CamKIIα-iCre male mice received infusion of hM3Dq or mCherry in the Ent. Three weeks later, mice began to receive daily administration of CNO for 5 weeks (Fig. 5k). Locomotor activity in hM3Dq-infused mice was similar to mCherry-infused mice when examined after 4 weeks of CNO treatment (Fig. 5l). However, in the novelty-suppressed feeding test performed after 5 weeks of CNO, hM3Dq-infused mice displayed a 47% shorter latency to feed versus mCherry-infused mice (Fig. 5m), suggesting an antidepressive-like effect. This was a specific effect, as after the novelty-suppressed feeding test, both hM3Dq- and mCherry-infused mice consumed the same amount of food in the home cage (Fig. 5n). In contrast to the antidepressive-like behaviors seen in hM3Dq mice after chronic CNO injections, hM3Dq- and

Fig. 5 | Chemogenetic stimulation of the Ent–DG circuit drives activity-dependent processes in the DG and antidepressive-like behavior. a, Timeline of experiments that used designer receptors exclusively activated by designer drugs (DREADDs) and examined cellular endpoints (c-Fos and neurogenesis measures). **b**, A schematic of stereotaxic Ent infusion of mCherry (control virus: AAV-hSyn-DIO-mCherry) or hM3Dq (CNO-dependent stimulation virus: AAV-hSyn-DIO-hM3Dq-mCherry) in CamKIIα-iCre mice that had received BrdU. **c**, A photomicrograph taken 4 weeks after Ent infusion and 4 weeks after daily i.p. injection of CNO showing that mCherry$^+$ terminals were evident in the DG molecular layer. Scale bar, 200 μm. **d**,**e**, Four weeks after mCherry or hM3Dq Ent infusion, daily i.p. injection of CNO led to more c-Fos$^+$ cells in the Ent (**d**, top) and the DG (**d**, bottom) but not in other hippocampal regions (**e**) in hM3Dq-infused mice relative to mCherry-infused mice. Scale bar, 200 μm. Statistical analysis was performed using a two-way ANOVA in **e**: effects of subregion, $F_{2,24}=6.065$, $P<0.01$; treatment, $F_{1,24}=2.442$, $P>0.05$; and bregma × treatment interaction, $F_{2,24}=4.221$, $P<0.05$. Bonferroni post hoc analysis was performed: $^*P<0.05$. $n=5$ mCherry-infused mice, 5 hM3Dq-infused mice. **f**, Photomicrographs showing DG BrdU$^+$ cells in mCherry- and hM3Dq-infused mice. Scale bar, 200 μm. **g**, Quantification of DG BrdU$^+$ cells in mCherry- and hM3Dq-infused mice. **h**, Quantification of DG BrdU$^+$ cells in specific positions relative to bregma in mCherry- and hM3Dq-infused mice. For **g** and **h**, $n=14$ mCherry-infused mice, 14 hM3Dq-infused mice. **i**, Photomicrographs showing DG BrdU$^+$NeuN$^+$ neurons in mCherry- and hM3Dq-infused mice. Scale bar, 20 μm. **j**, Quantification of the number of DG BrdU$^+$NeuN$^+$ neurons in mCherry- and hM3Dq-infused mice. $n=5$ mCherry-infused mice, 5 hM3Dq-infused mice. Statistical analysis was performed using an unpaired *t*-test in **g** and **j**: $^{**}P<0.01$, $^{***}P<0.001$; a two-way ANOVA was used in **h**: effects of bregma, $F_{13,364}=27.90$, $P<0.0001$; treatment, $F_{1,364}=51.07$, $P<0.0001$; and bregma × treatment interaction, $F_{13,364}=2.901$, $P<0.001$. Bonferroni post hoc analysis was performed for treatment in **h**: *a*, $P<0.05$; *a′*, $P<0.01$; *a″* $P<0.001$. **k**, The timeline of studies on behavior induced by chronic chemogenetic stimulations. **l**, hM3Dq-infused mice had similar locomotor activity (time of day shown on *x* axis) relative to mCherry-infused mice before and after daily chronic CNO injection. Statistical analysis was performed using a two-way repeated-measures ANOVA in **l**: effects of time, $F_{79,1580}=10.75$, $P<0.0001$; treatment, $F_{1,20}=0.7316$, $P>0.05$; subjects, matching, $F_{20,1580}=3.971$, $P<0.0001$; and time × treatment interaction, $F_{79,1580}=0.2065$, $P>0.9999$. **m**,**n**, hM3Dq-infused mice had a shorter latency to feed in the novelty-suppressed feeding test than the mCherry-infused mice (**m**), but food consumption in the home cage was similar between the groups (**n**). For **l**–**n**, $n=8$ mCherry-infused mice, 7 hM3Dq-infused mice. Statistical analysis with an unpaired *t*-test was used in **m** and **n**: $^*P<0.05$. **o**, The timeline of studies on behavior induced by acute chemogenetic stimulation. **p**, hM3Dq-infused mice had similar locomotor activity (time of day shown on *x* axis) relative to mCherry-infused mice before and after CNO injection. Statistical analysis was performed using a two-way repeated-measures ANOVA in **p**: effects of time, $F_{79,1106}=14.82$, $P<0.0001$; treatment, $F_{1,14}=0.7466$, $P>0.05$; subjects, matching, $F_{14,1106}=9.23$, $P<0.0001$; and time × treatment interaction, $F_{79,1106}=0.7006$, $P>0.05$. **q**,**r**, hM3Dq- and mCherry-infused mice had a similar latency to feed in the novelty-suppressed feeding test (**q**) and similar food consumption in the home cage (**r**). Statistical analysis was performed using an unpaired *t*-test in **q** and **r**; $P>0.05$. For **p**–**r**, $n=7$ mCherry-infused mice, 9 hM3Dq-infused mice. **s**, The timeline of CSDS. **t**, Ten days of CSDS decreased the time of SI in mCherry-infused mice relative to mCherry-infused control mice. However, chronic stimulation of the Ent in hM3Dq mice increased the time of SI relative to mCherry-infused mice that received CSDS. $n=6$ mCherry/Control mice, 6 hM3Dq/Control mice, 16 mCherry/CSDS mice, 12 hM3Dq/CSDS mice. A two-way repeated-measures ANOVA was used for statistical analysis in **t**: effects of target, $F_{1,36}=7.494$, $P<0.01$; virus, $F_{3,36}=3.155$, $P<0.05$; subjects, matching, $F_{36,36}=2.242$, $P<0.01$; and target × virus interaction, $F_{3,36}=2.132$, $P>0.05$. Fisher's LSD post hoc analysis was performed for virus: $^*P<0.05$, $^{**}P<0.01$. Data are shown as mean ± s.e.m. in **e**, **g**, **h**, **j**, **l**–**n**, **p**–**r**, and **t** with data points from individual mice in **e**, **g**, **j**, **m**, **n**, **q**, **r**, and **t**. See Supplementary Table 1 and the Life Sciences Reporting Summary for detailed statistical information.

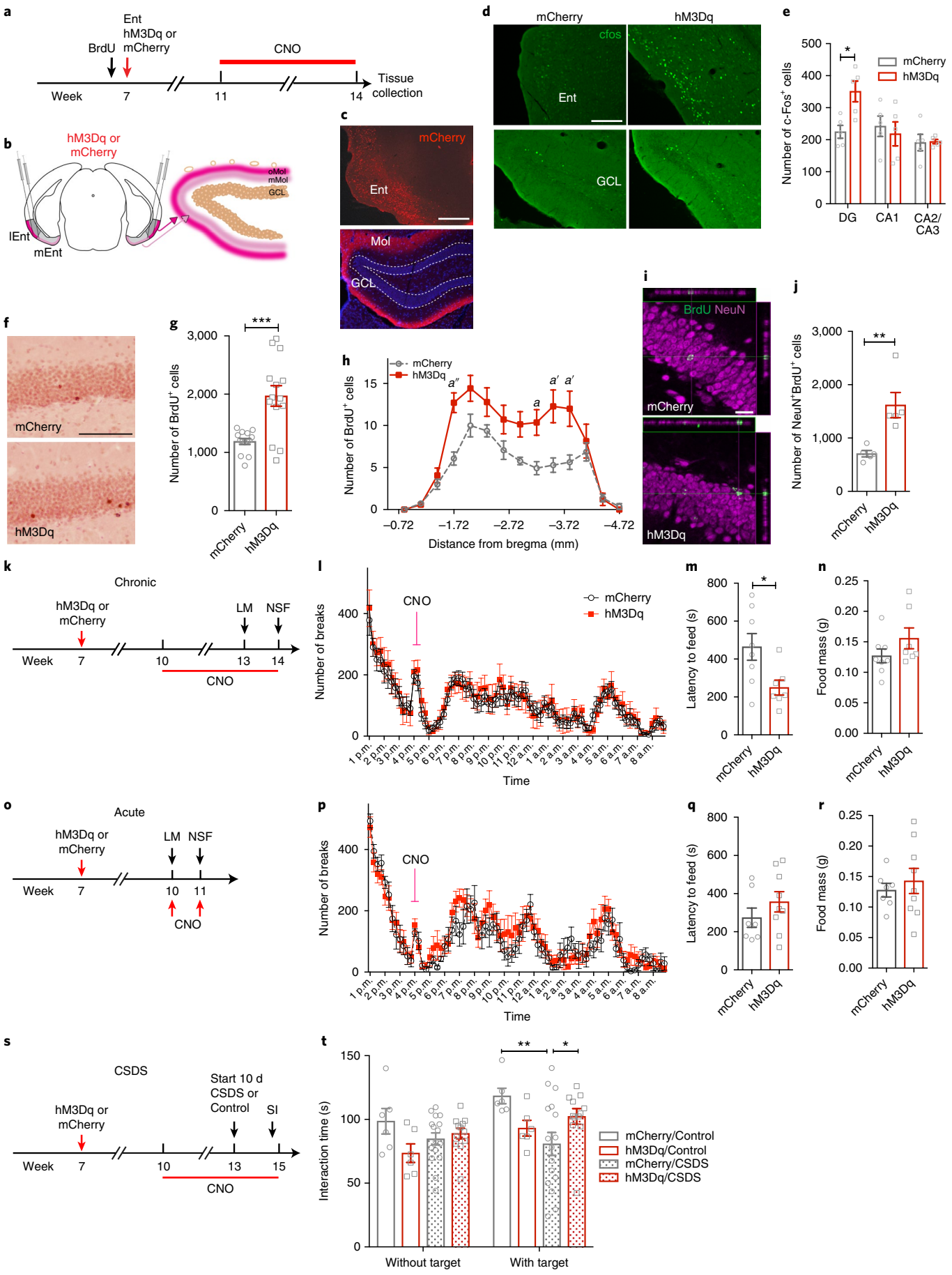

mCherry-infused male mice that were given an acute CNO treatment (2 mg/kg) 3 weeks following viral infusion (Fig. 5o) showed similar locomotor behavior and latency to feed (Fig. 5p–r).

Finally, we hypothesized that chronic stimulation of glutamatergic afferents from the Ent to the DG would enhance antidepressive-like behavior under conditions of an ethologically relevant chronic social stress, such as CSDS[18,36,37]. To test this hypothesis, 7-week-old CamKIIα-iCre male mice received Ent infusion of hM3Dq or mCherry, began to receive daily CNO injections 3 weeks after viral infusion, and began 10 d of CSDS or control housing (housed in partitioned cage with conspecific instead of aggressor) 4 weeks into the CNO regimen (Fig. 5s). SI testing revealed that, although there were no differences among groups when a social target was absent (Fig. 5t), mCherry-infused mice that underwent CSDS had less interaction with a social target than nonstressed mCherry-infused mice, as expected. In addition, hM3Dq-infused mice that underwent CSDS had more interaction time with a social target than mCherry-infused mice that underwent CSDS (Fig. 5t). Taken together, our findings show that stimulation of glutamatergic neurons in the Ent–DG circuit is antidepressive, even in an animal model of stress-induced depression.

Discussion

The Ent–hippocampal circuit is well-known for its role in processing episodic memory of spatial and object information[38,39], and recent research shows that Ent stimulation has physiological benefits in learning- and memory-related processes in humans. For example, in humans, Ent DBS enhances spatial learning and is accompanied by resetting of hippocampal theta rhythms[8]. In contrast, direct DBS of the human hippocampus either does not affect or negatively influences hippocampal-dependent memory[8,40], emphasizing the utility of targeting hippocampal input rather than the hippocampus itself. In addition to this work in humans, preclinical work also supports the idea that DBS of the Ent improves spatial learning and memory, specifically driving activity-dependent adult neurogenesis in the mouse hippocampus[7]. Our present work supports this, as we show stimulation of Ent–DG circuitry in mice improves hippocampal-dependent memory. However, our main goal was to test the new hypothesis that Ent stimulation would be effective in ameliorating depressive-like behaviors. This hypothesis was inspired by the Ent and hippocampal structural deficits seen in the brains of humans with MDD and in animal models of depression[4,5,9] and by the ability of many antidepressant drugs and even nonpharmacological treatments, like ECT, to ameliorate these structural deficits[41–43]. In support of our hypothesis, we show both molecular- and chemogenetic-based stimulation of Ent–DG circuitry in mice combats stress-induced depressive-like behavior. For any new therapeutic, it is critical to consider the intensity and duration of treatment. Interestingly, prior work showed longer-term—but not acute—Ent DBS improved learning- and memory-related function of the hippocampus[7,8,40]. Our present work also shows that chronic—but not acute—Ent stimulation drives antidepressive-like behaviors in mice. It remains to be tested how long the Ent-stimulation-induced memory enhancement and antidepressive-like behavior persist. Importantly, it also remains unknown whether Ent stimulation will alleviate MDD symptoms in humans. However, our findings in laboratory mice emphasize the power and potential of Ent glutamatergic afferent stimulation—previously known for the ability to positively influence learning and memory—for the treatment of MDD.

In light of the efficacy of Ent stimulation for both the alleviation of stress-induced depressive-like behavior in mice described here and for improvement of learning- and memory-related processes in both mice and humans[7,8], it is notable that many psychiatric disorders (MDD, bipolar disorder, schizophrenia, post-traumatic stress disorder, and substance-use disorders) share symptoms reminiscent of abnormal DG function: dysregulated memory, mood regulation, pattern separation, and reward processing. Future studies are warranted to examine whether Ent stimulation broadly normalizes DG function and thus ameliorates symptoms in other disorders aside from MDD. In addition, given the functional heterogeneity of the mammalian hippocampus[44], it will be important to assess whether targeting subregions of the Ent results in specific functional outcomes or whether the entire perforant path needs to be engaged. This is particularly true considering that anxiety-like behaviors rely on both the dorsal and ventral DG[44]. Also, it remains unknown whether the functions of the DG closely relate to each other, such that improvement in mood regulation, for example, also improves memory. A corollary of this is whether or not Ent stimulation will improve DG functions that are far less studied, such as contextual pattern separation and reward processing. For example, disruption of Ent via excitotoxic lesion also disrupts pattern separation[45], and an inducible increase of adult DG neurogenesis improves pattern separation[46], but it remains to be seen whether stimulation of the Ent–DG circuit improves pattern separation.

Mechanistically, we show that Ent-stimulation-induced antidepressive-like behavior relies on intact DG neurogenesis. These data are in line with causative studies in mice showing newly generated DG neurons are required for antidepressant efficacy, particularly under stressful conditions[24,35,47]. Although 'increased hippocampal neurogenesis' has been proposed to even underlie the effectiveness of certain antidepressants[48,49], it has thus far been unclear how this action was achieved. Our results showing that stimulation of Ent–DG circuitry spurs adult hippocampal neurogenesis and drives antidepressant behavior raise the possibility that these actions could be harnessed to improve mood more effectively and/or enhance resilience in the face of stressful situations.

Our findings provide the first evidence to our knowledge that the Ent–DG circuit may be targeted for depression treatment, with chronic—but not acute—stimulation driving antidepressive-like behaviors. The ability to produce antidepressive-like behaviors by stimulating the Ent–DG circuitry fits well with the modern framing of depression as a circuitopathy[50]. As stimulation of the Ent–DG circuitry enhances hippocampal function relevant to mood and memory, targeting this new circuit for MDD treatment may preclude side effects of currently employed brain stimulation therapies (i.e., memory loss and cognitive impairment) and will address the great demand for new avenues of treatment for humans who are affected by MDD.

Methods

Methods, including statements of data availability and any associated accession codes and references, are available at https://doi.org/10.1038/s41591-018-0002-1.

Received: 13 March 2016; Accepted: 26 January 2018;
Published online: 16 April 2018

References

1. Kupfer, D. J., Frank, E. & Phillips, M. L. Major depressive disorder: new clinical, neurobiological, and treatment perspectives. *Lancet* **379**, 1045–1055 (2012).
2. Trivedi, M. H. Modeling predictors, moderators and mediators of treatment outcome and resistance in depression. *Biol. Psychiatry* **74**, 2–4 (2013).
3. Rosa, M. A. & Lisanby, S. H. Somatic treatments for mood disorders. *Neuropsychopharmacology* **37**, 102–116 (2012).
4. Kronmüller, K.-T. et al. Hippocampal volume and 2-year outcome in depression. *Br. J. Psychiatry* **192**, 472–473 (2008).
5. Yun, S., Reynolds, R. P., Masiulis, I. & Eisch, A. J. Re-evaluating the link between neuropsychiatric disorders and dysregulated adult neurogenesis. *Nat. Med.* **22**, 1239–1247 (2016).
6. Miller, B. R. & Hen, R. The current state of the neurogenic theory of depression and anxiety. *Curr. Opin. Neurobiol.* **30**, 51–58 (2015).
7. Stone, S. S. D. et al. Stimulation of entorhinal cortex promotes adult neurogenesis and facilitates spatial memory. *J. Neurosci.* **31**, 13469–13484 (2011).

8. Suthana, N. et al. Memory enhancement and deep-brain stimulation of the entorhinal area. *N. Engl. J. Med.* **366**, 502–510 (2012).
9. Gerritsen, L. et al. Depression, hypothalamic pituitary adrenal axis, and hippocampal and entorhinal cortex volumes—the SMART Medea study. *Biol. Psychiatry* **70**, 373–380 (2011).
10. Biel, M., Wahl-Schott, C., Michalakis, S. & Zong, X. Hyperpolarization-activated cation channels: from genes to function. *Physiol. Rev.* **89**, 847–885 (2009).
11. Lewis, A. S. et al. Deletion of the hyperpolarization-activated cyclic nucleotide-gated channel auxiliary subunit TRIP8b impairs hippocampal Ih localization and function and promotes antidepressant behavior in mice. *J. Neurosci.* **31**, 7424–7440 (2011).
12. Santoro, B. et al. TRIP8b splice variants form a family of auxiliary subunits that regulate gating and trafficking of HCN channels in the brain. *Neuron* **62**, 802–813 (2009).
13. Lewis, A. S. et al. Alternatively spliced isoforms of TRIP8b differentially control h channel trafficking and function. *J. Neurosci.* **29**, 6250–6265 (2009).
14. Kim, C. S., Chang, P. Y. & Johnston, D. Enhancement of dorsal hippocampal activity by knockdown of HCN1 channels leads to anxiolytic- and antidepressant-like behaviors. *Neuron* **75**, 503–516 (2012).
15. Urban, D. J. & Roth, B. L. DREADDs (designer receptors exclusively activated by designer drugs): chemogenetic tools with therapeutic utility. *Annu. Rev. Pharmacol. Toxicol.* **55**, 399–417 (2015).
16. Fanselow, M. S. & Dong, H.-W. Are the dorsal and ventral hippocampus functionally distinct structures? *Neuron* **65**, 7–19 (2010).
17. Sahay, A. & Hen, R. Adult hippocampal neurogenesis in depression. *Nat. Neurosci.* **10**, 1110–1115 (2007).
18. Krishnan, V. et al. Molecular adaptations underlying susceptibility and resistance to social defeat in brain reward regions. *Cell* **131**, 391–404 (2007).
19. Kourrich, S., Glasgow, S. D., Caruana, D. A. & Chapman, C. A. Postsynaptic signals mediating induction of long-term synaptic depression in the entorhinal cortex. *Neural Plast.* **2008**, 840374 (2008).
20. Latchney, S. E., Jiang, Y., Petrik, D. P., Eisch, A. J. & Hsieh, J. Inducible knockout of Mef2a, -c, and -d from nestin-expressing stem/progenitor cells and their progeny unexpectedly uncouples neurogenesis and dendritogenesis in vivo. *FASEB J.* **29**, 5059–5071 (2015).
21. Guo, W. et al. Ablation of Fmrp in adult neural stem cells disrupts hippocampus-dependent learning. *Nat. Med.* **17**, 559–565 (2011).
22. Petrik, D., Lagace, D. C. & Eisch, A. J. The neurogenesis hypothesis of affective and anxiety disorders: are we mistaking the scaffolding for the building? *Neuropharmacology* **62**, 21–34 (2012).
23. Hill, A. S., Sahay, A. & Hen, R. Increasing adult hippocampal neurogenesis is sufficient to reduce anxiety and depression-like behaviors. *Neuropsychopharmacology* **40**, 2368–2378 (2015).
24. Snyder, J. S., Soumier, A., Brewer, M., Pickel, J. & Cameron, H. A. Adult hippocampal neurogenesis buffers stress responses and depressive behaviour. *Nature* **476**, 458–461 (2011).
25. Walker, A. K. et al. The P7C3 class of neuroprotective compounds exerts antidepressant efficacy in mice by increasing hippocampal neurogenesis. *Mol. Psychiatry* **20**, 500–508 (2015).
26. David, D. J. et al. Neurogenesis-dependent and -independent effects of fluoxetine in an animal model of anxiety/depression. *Neuron* **62**, 479–493 (2009).
27. Stone, E. A. & Lin, Y. An anti-immobility effect of exogenous corticosterone in mice. *Eur. J. Pharmacol.* **580**, 135–142 (2008).
28. Gourley, S. L. et al. Regionally specific regulation of ERK MAP kinase in a model of antidepressant-sensitive chronic depression. *Biol. Psychiatry* **63**, 353–359 (2008).
29. Murray, F., Smith, D. W. & Hutson, P. H. Chronic low dose corticosterone exposure decreased hippocampal cell proliferation, volume and induced anxiety and depression like behaviours in mice. *Eur. J. Pharmacol.* **583**, 115–127 (2008).
30. White, W. F., Nadler, J. V., Hamberger, A., Cotman, C. W. & Cummins, J. T. Glutamate as transmitter of hippocampal perforant path. *Nature* **270**, 356–357 (1977).
31. Melzer, S. et al. Long-range-projecting GABAergic neurons modulate inhibition in hippocampus and entorhinal cortex. *Science* **335**, 1506–1510 (2012).
32. Casanova, E. et al. A CamKIIα iCre BAC allows brain-specific gene inactivation. *Genesis* **31**, 37–42 (2001).
33. Krashes, M. J. et al. An excitatory paraventricular nucleus to AgRP neuron circuit that drives hunger. *Nature* **507**, 238–242 (2014).
34. Vismer, M. S., Forcelli, P. A., Skopin, M. D., Gale, K. & Koubeissi, M. Z. The piriform, perirhinal, and entorhinal cortex in seizure generation. *Front. Neural Circuits* **9**, 27 (2015).
35. Santarelli, L. et al. Requirement of hippocampal neurogenesis for the behavioral effects of antidepressants. *Science* **301**, 805–809 (2003).
36. Lagace, D. C. et al. Adult hippocampal neurogenesis is functionally important for stress-induced social avoidance. *Proc. Natl. Acad. Sci. USA* **107**, 4436–4441 (2010).
37. Russo, S. J., Murrough, J. W., Han, M.-H., Charney, D. S. & Nestler, E. J. Neurobiology of resilience. *Nat. Neurosci.* **15**, 1475–1484 (2012).
38. Eichenbaum, H. A cortical–hippocampal system for declarative memory. *Nat. Rev. Neurosci.* **1**, 41–50 (2000).
39. Tulving, E. Episodic memory: from mind to brain. *Annu. Rev. Psychol.* **53**, 1–25 (2002).
40. Jacobs, J. et al. Direct electrical stimulation of the human entorhinal region and hippocampus impairs memory. *Neuron* **92**, 983–990 (2016).
41. Surget, A. et al. Antidepressants recruit new neurons to improve stress response regulation. *Mol. Psychiatry* **16**, 1177–1188 (2011).
42. Ma, D. K. et al. Neuronal activity–induced Gadd45b promotes epigenetic DNA demethylation and adult neurogenesis. *Science* **323**, 1074–1077 (2009).
43. Boldrini, M. et al. Hippocampal angiogenesis and progenitor cell proliferation are increased with antidepressant use in major depression. *Biol. Psychiatry* **72**, 562–571 (2012).
44. Kheirbek, M. A. et al. Differential control of learning and anxiety along the dorsoventral axis of the dentate gyrus. *Neuron* **77**, 955–968 (2013).
45. Vivar, C. et al. Monosynaptic inputs to new neurons in the dentate gyrus. *Nat. Commun.* **3**, 1107 (2012).
46 Sahay, A. et. al. Increasing adult hippocampal neurogenesis is sufficient to improve pattern separation. *Nature* **472**, 466–470 (2011).
47. Airan, R. D. et al. High-speed imaging reveals neurophysiological links to behavior in an animal model of depression. *Science* **317**, 819–823 (2007).
48. Crupi, R., Marino, A. & Cuzzocrea, S. New therapeutic strategy for mood disorders. *Curr. Med. Chem.* **18**, 4284–4298 (2011).
49. Malberg, J. E. & Schechter, L. E. Increasing hippocampal neurogenesis: a novel mechanism for antidepressant drugs. *Curr. Pharm. Des.* **11**, 145–155 (2005).
50. Lozano, A. M. & Lipsman, N. Probing and regulating dysfunctional circuits using deep brain stimulation. *Neuron* **77**, 406–424 (2013).

Acknowledgements

We thank S. G. Birnbaum, I. M. Bowen, L. Peca, S. Stojadinovic, and Z. Zhang for assistance in experimental techniques. We thank E. D. Marsh and A. J. McCoy for guidance on use of computer code. We thank C. A. Tamminga and J. M. Zigman for sharing animals and tissues that were useful for pilot experiments. We thank G. A. Barr, I. M. Bowen, and S. E. Latchney for helpful discussions and feedback. This work was supported by grants from the National Institutes of Health to A.J.E. (DA023701, DA023555, MH107945) and D.M.C. (NS059934, MH104471), the National Aeronautics and Space Administration to A.J.E. (NNX07AP84G, NNX12AB55G, NNX15AE09G) and an Independent Investigator Award from the National Alliance for Research on Schizophrenia and Depression/Brain and Behavior Foundation to A.J.E. S.Y. was funded by a National Institute of Mental Health Basic Science Institutional NRSA Training Grant (Training Program in the Neurobiology of Mental Illness,T32-MH076690, principal investigator: C. A. Tamminga). P.D.R. was funded by National Institute on Drug Abuse NRSA Institutional Training Grant (Basic Science Training Program in the Drug Abuse Research, T32-DA007290, principal investigator: A. J. Eisch).

Author contributions

S.Y. conceived the study, performed most experiments, generated the figures, and wrote the manuscript. R.P.R. assisted with experiments and generated figure schematics. I.P. and A.W. performed EEG experiments. A.S. and S.K. performed the electrophysiology experiments. P.D.R., A.D.G., M.S., M.J.D., N.I., S.M., D.R.R., and I.S. assisted with experiments. C.E.K. and D.M.C. provided *Trip8b* knockout mouse brains and TRIP8b-specific and TRIP8b-isoform-specific antibodies (Northwestern University). R.C.A.-N. wrote the code for the in vivo EEG experiment analysis (Children's Hospital of Philadelphia Research Institute). D.A.C. guided the EEG experiments. A.J.E. conceived the study, assisted with experiments, guided figure preparation, and wrote the manuscript.

Competing interests

The authors declare no competing interests.

Additional information

Supplementary information is available for this paper at https://doi.org/10.1038/s41591-018-0002-1.

Reprints and permissions information is available at www.nature.com/reprints.

Correspondence and requests for materials should be addressed to A.J.E.

Publisher's note: Springer Nature remains neutral with regard to jurisdictional claims in published maps and institutional affiliations.

Methods

Mice and ethics statement. Experiments were approved by the Institutional Animal Use and Care Committee at the University of Texas Southwestern Medical Center (UTSW; APN 0960-07-02-1 and 2015-100851) and at the Children's Hospital of Philadelphia (Penn Medicine–CHOP; APN IAC-17-001245). Mice were group-housed in a UTSW or CHOP vivarium accredited by the Association for Assessment and Accreditation of Laboratory Animal Care (AAALAC), unless otherwise noted, and were kept on a 12-h light–dark cycle with ad libitum access to food and water. 7- or 8-week old C57BL/6 J male or female mice were purchased from Jackson Laboratory (stock number: 000664). nestin-GFP mice were bred at UTSW, and CamKIIα-iCre mice were bred at UTSW and CHOP[32,51]. *Trip8b* germline knockout mice were generated at the Chetkovich Laboratory[11] by breeding heterozygous *Trip8b*$^{+/-}$ mice with one another. Mice were genotyped through PCR using genomic DNA and previously published primers[11,32]. All experiments were performed in compliance with local and national guidelines on the care and use of animals.

Adeno-associated virus vectors, virus production and virus purification. shRNAs were designed to target the TRIP8b C-terminus region (exon 11), as previously published[13]. The following oligonucleotides with overhanging ends identical to those created by SapI and XbaI restriction enzymes were used: TRIP8b shRNA, 5′-TTTGAGCATTTGAAGAAGGCTTAATTCAAGAGATTAAGCCTT CTTCAAAT GCTATTTTT-3′; SCR shRNA, 5′-TTTGTTCTCCGAACGT GTCACGTTTCAAGAGAACGTGACACGTTCGGAGAATTTTT-3′. Hairpin oligonucleotides were phosphorylated using T4 polynucleotide kinase (New England Biolabs, Beverly, MA) followed by annealing at 100 °C for 5 min and cooling in the heat block for 3 h. Each annealed oligonucleotide was ligated into the AAV_2 plasmid (pAAV-EGFP-shRNA; Stratagene, La Jolla, CA). Viruses were attained either through production using helper-free triple transfection in HEK293T cells (American Type Culture Collection, VA), with purification as previously described[52,53] in the laboratory, or through purchase from University of Pennsylvania Vector core. AAV_8-hSyn-DIO-hM3Dq-mCherry and AAV_8-hSyn-DIO-mCherry viruses were purchased from the University of North Carolina Vector Core Facilities (Chapel Hill, NC). The virus titer was approximately 1.9×10^{12} vg/ml.

Stereotaxic injection. Mice were anesthetized with a mixture of ketamine (120 mg/kg) and xylazine (16 mg/kg) in saline (0.9% NaCl, i.p.). Bilateral stereotaxic injection of 0.4 to 0.5 µl of purified high-titer AAV (TRIP8b shRNA, SCR shRNA, hM3Dq, or mCherry) was directed into the lEnt (injection coordinates from bregma: anterior/posterior (A/P) −3.7 mm, medial/lateral (M/L) + 4.4 mm, angle 4°; from lambda: dorsal/ventral (D/V) −4.5 mm) and mEnt (injection coordinates from bregma: A/P −3.9 mm, M/L + 3.9 mm, angle 4°; from lambda: D/V −4.5 mm) using 33-gauge Hamilton syringes (Hamilton, Reno, NV). The injection rate was 0.1 µl/min, with needles kept in place for an additional 5 min to enable diffusion. Mice were randomly allocated to experimental or control groups. Accurate virus targeting (EGFP$^+$ or mCherry$^+$ soma in Ent II/III and EGFP$^+$ or mCherry$^+$ terminals in the perforant path and the middle and/or outer DG molecular layer; Supplementary Figs. 5 and 10) was verified after brain collection. Data from mice in which labeled terminals were seen in CA1 or CA3 (stratum oriens, SO; stratum pyramidalis, SP; or stratum radiatum, SR), subiculum (Sub) or amygdala (Amyg) were excluded from the cellular and behavioral analyses in the main text. In mice with strong terminal expression in the DG molecular layer, immunohistochemistry with amplification and high magnification revealed fine projections in the stratum lacunosum-moleculare (SLM). The cellular and behavioral data for these mice are also included in the main text if EGFP$^+$ or mCherry$^+$ terminals were not detected in other CA1 regions (SO, SP, SR). Data from mice in which the viral infusion was mistargeted (not centered in the Ent and terminal expression outside of expected downstream regions) were analyzed to confirm the lack of antidepressive-like behavior with off-target TRIP8b shRNA animals (Supplementary Fig. 5).

Drug administration. Mice were injected twice (6-h interinjection interval) with BrdU (Roche Applied Sciences Indianapolis, IN, made as 10 mg/ml in 0.9% saline, injected i.p. as 15 ml/kg) at a dose of 150 mg/kg[54] 24 h before stereotaxic surgery to label dividing cells and eventually quantify surviving BrdU immunoreactive (BrdU$^+$) cells. Female C57BL/6 J mice that received Ent stereotaxic infusion of virus (AAV_2-TRIP8b shRNA or AAV_2-SCR shRNA) were given oral corticosterone (Sigma-Aldrich, cat. no. C2505, 7.5 mg/kg/day, stock solution 52.5 µg/ml), dissolved in 0.3% EtOH in 0.45% 2-hydroxypropyl-β-cyclodextrin (vehicle, Sigma-Aldrich, cat. no. H107)[23,26] in opaque bottles to protect the solution from light, that was available ad libitum in the drinking water for 7 weeks. Male CamKIIα-iCre mice in which the Ent was infused with virus (AAV_8-hSyn-DIO-hM3Dq-mCherry or AAV_8-hSyn-DIO-mCherry) were injected with CNO (National Institute of Mental Health Chemical Synthesis and Drug Supply Program) dissolved in 0.5% DMSO (Calbiochem, cat. no. 317275) in 0.9% saline[33]. The dose of CNO was as follows: CSDS experiments, 1 mg/kg of 0.2 mg/ml solution, i.p. daily for 6 weeks; non-CSDS chronic and acute DREADD behavior and cellular experiments, 2 mg/kg of 0.2 mg/ml solution, i.p. daily for 4 to 5 weeks (chronic) or 1 injection before each behavioral test (acute); EEG experiments, 1 mg/kg of 0.2 mg/ml solution i.p daily for 5 weeks and then either 1 mg/kg of 0.2 mg/ml solution (low dose) or 10 mg/kg (high dose) of 1 mg/ml solution during EEG monitoring.

Electrophysiology. Horizontal slices (300 µm) to be used for whole-cell current-clamp patch recording of neurons in Ent layer II were prepared as described previously[19] and according to timeline shown in Fig. 2f. Slices recovered in a holding chamber for ~1 h before use. During recording, slices were superfused with artificial cerebrospinal fluid (ACSF; 31.5–32.5 °C) saturated with 95% O_2 and 5% CO_2 and containing 119 mM NaCl, 2.5 mM KCl, 1.0 mM NaH_2PO_4, 1.3 mM $MgSO_4$, 2.5 mM $CaCl_2$, 26.2 mM $NaHCO_3$, and 11 mM glucose. During recordings, ACSF-containing picrotoxin (100 mM) was used to block $GABA_A$ receptor–mediated inhibitory postsynaptic potentials, and kynurenic acid (2 mM) was used to block glutamate receptors. All recordings were performed on stellate neurons in Ent layer II. Layer II neurons were classified as stellate or nonstellate neurons on the basis of electrophysiological characteristics described previously[55]. Briefly, stellate neurons were characterized by the presence of low-frequency, subthreshold membrane potential oscillations, a depolarizing afterpotential following spikes, and prominent inward rectification in response to hyperpolarizing current pulses. To quantify firing properties, whole-cell current-clamp recordings were performed with electrodes (3–5 MΩ) containing 120 mM K-gluconate, 20 mM KCl, 10 mM HEPES, 0.2 mM EGTA, 2 mM $MgCl_2$, 4 mM MgATP, and 0.3 mM NaGTP at a pH of 7.20–7.25. Data were filtered at 5 KHz, digitized at 10 KHz, and collected and analyzed via Clampex 10.3.0.2 (Molecular Devices, Inc.). Membrane potentials were maintained at −70 mV. Series resistances (10–18 MΩ) and input resistances (R_i) were monitored on-line with a 40 pA current injection (150 ms) given before each 700-ms current injection stimulus. Only cells with a stable R_i (change < 10%) for the duration of the recording were kept for analysis. The firing rate for a given cell was the average value measured from 2 to 4 cycles (duration: 700 ms at 0.1 Hz, range: −320 to + 320 pA, increment: 40-pA step).

Electroencephalogram recordings. EEG monitoring was performed as previously described[56] and according to timeline shown in Fig. 2i. Mice were stereotaxically implanted with an electrode assembly under continuous isoflurane anesthesia. The electrode assembly consisted of six channels: two surface electrodes attached to miniature skull screws placed over the left and right frontal cortices (from bregma: A/P −1.2 mm, M/L ± 1.1 mm); a double-depth electrode in right hippocampus (from bregma: A/P −2.2 mm, M/L + 1.2 mm, D/V −1.3 mm; and finally a reference and a ground electrode directly behind lambda on either side of midline. Teflon-coated silver wires (0.13-mm diameter) were attached to each electrode and connected to a 6-pin pedestal (Plastics One, Roanoke, VA). The entire assembly was secured on the skull with dental cement (Ortho-Jet, LangDental, Wheeling, IL). A flexible cable connected the headcap assembly for each mouse to a commutator, thus allowing the mouse to move freely during the recordings. Mice were given ≥72 h postsurgery to recover before the being placed in recording cage and were acclimatized for ≥24 h in recording cage before recording initiation. Video-monitored EEG recordings of awake and behaving mice were performed in custom-made Plexiglas cages using a Stellate Harmonie acquisition interface (Natus Medical, Pleasanton, CA) and sampled at 2 kHz.

EEG signals were processed offline for the detection of seizures and for the purpose of power spectral density analyses. Seizures were detected manually through inspection of EEG traces. Power spectra analyses were performed using NeuroExplorer (ver. 5, Nex Technologies, Madison, AL) in conjunction with a custom-made MatLab code. Frequency bands were separated into delta (0.1–4 Hz), theta (4.1–8 Hz), alpha (8.1–13 Hz), beta (13.1–25 Hz), and gamma (25.1–50 Hz) ranges. The relative power for each frequency band was calculated through dividing the absolute power for each frequency by the total power and then normalizing it with a log transformation to allow for comparisons between mice.

Data were analyzed separately for the day and night cycles (lights on, 6:15 a.m.; lights off, 6:15 p.m.). Furthermore, for the effects of CNO, data were sampled and analyzed between 90 and 360 min following CNO administration. Given that CNO was injected at 3:15 p.m. on days of administration, data collected following CNO treatment were further segregated into daytime and nighttime segments. In summary, data were analyzed for TRIP8b-shRNA-infused and SCR-shRNA-infused mice during daytime and nighttime, and for hM3Dq-infused and mCherry-infused mice during daytime pre-CNO, daytime post-CNO, and nighttime post-CNO. For the model of pilocarpine-induced epilepsy, 6- to 8-week-old C57BL/6 mice were injected with scopolamine (1 mg/kg, i.p.) and, 30 min later, with pilocarpine (315 mg/kg, i.p.), which typically triggers seizure activity (status epilepticus) within <30 min[57]. Sixty minutes after status epilepticus onset, diazepam (5 mg/kg, i.p.) was administered to quell seizure activity. Mice were left to recover for at least 2 weeks before they were surgically implanted with EEG electrode assemblies as described above. In pilocarpine-treated mice, spontaneous electrographic and/or behavioral seizures typically start manifesting within 8–15 d following status epilepticus[57], and the recordings presented here were collected ~1 month following pilocarpine treatment. Data for power analyses were sampled in the form of 10 pseudorandomly selected, noise- and artifact-free, 2-min epochs for each designated time period (see above) for each day of recording. The relative power values for these 10 epochs were subsequently averaged, resulting in a single relative power value for each time period for each day. When data were collected

across multiple days, data from multiple days were averaged for each designated time period. Experimenters remained blind throughout quantification and analysis of data.

Image-guided cranial irradiation. Image-guided cranial irradiation was delivered via the X-RAD 225Cx self-contained irradiation system (Precision X-Ray) as previously published[25,58]. Briefly, 8-week-old male C57BL/6J mice were anesthetized with 1.5–2.5% isoflurane. Mice received diagnostic imaging to align the body and bregma coordinates with the collimator (6 mm × 14 mm rectangular collimator) to ensure hippocampal targeting. Mice then received image-guided cranial irradiation (10 Gy, 225 Kv, 13 mA, 207 s). Control mice (sham) were handled in the same manner as irradiated mice (for example, exposed to isoflurane for the same period of time), except they were not placed in the irradiator.

Tissue collection and western blot. Brains and adrenal glands from decapitated mice were immediately dissected and frozen on dry ice (Fig. 1). Supplementary Fig. 3h includes data only from mice with successful bilateral extraction of adrenal glands. For western blot quantification of the levels of TRIP8b isoforms, brains were sectioned coronally at 300 µm using a cryostat (Leica) through the A/P length of the hippocampus[59]. The hippocampal DG (distance range from bregma: –1.34 mm to –2.54 mm) was sampled (0.8-mm diameter punch, Fine Science Tools, Foster City, CA), and tissues were homogenized in RIPA Buffer (150 mM NaCl, 1% NP-40, 0.5% deoxycholic acid, 0.1% SDS, and 50 mM TRIS, pH 8.0) with protease inhibitors (Roche, Indianapolis, IN). Protein concentration was determined using the BCA Protein Assay Reagent (Pierce, Rockford, IL). 20 µg of protein was electrophoretically separated on a 7.5% Tris-acetate gel and transferred to nitrocellulose membranes (Millipore, Billerica, MA). After transferring proteins from gel to nitrocellulose membrane, membranes were horizontally cut to enable immunoblotting for proteins on subsections of membrane. Membranes were incubated with primary antibodies against rabbit anti-TRIP8b (total, from D.M.C.), guinea pig anti-TRIP8b (1a5, from D.M.C.), mouse anti-TRIP8b (exon 4, Neuromab, cat. no. 73-208), mouse anti-TRIP8b (1b, Neuromab, cat. no. 73-245), or mouse anti-GAPDH (Millipore, cat. no. MAB374). Appropriate HRP-conjugated donkey anti–rabbit IgG (Calbiochem, cat. no. 401393), HRP-conjugated donkey anti–guinea pig IgG (Jackson ImmunoResearch Laboratories, cat. no. 106-035-003), and HRP-conjugated donkey anti–mouse IgG secondary antibodies (Calbiochem, cat. no. 401253) were used. Immunoreactive proteins were detected via chemiluminescent substrate (Thermofisher Scientific, cat. no. 34077) using X-ray film (Phenix Research Product, cat. no. F-BX810). Stripping and reprobing was used only for the membrane subsection blotted first for IsoA5 and subsequently for TRIP8b. Stripping of IsoA5 was performed using Restore Western Blot Stripping Buffer (Thermo Fisher Scientific, cat. no. 21059) following the manufacturer's instructions, and the blot was then incubated with anti-TRIP8b antibody (total, from D.M.C.). Images of immunoreactive bands were captured using a 3CCD color video camera (Sony, cat. no. DCX-3900), and the intensities were analyzed through densitometry using Scion image software (Scion Corporation). The measurements of immunoreactivity for each protein of interest were normalized to GAPDH in each sample.

To test the efficiency of in vitro TRIP8b knockdown, HEK293T cells were cotransfected with a plasmid expressing TRIP8b including exon 1a and exon 4 (from D.M.C.) and either pAAV-SCR-shRNA-EGFP or pAAV-TRIP8b-shRNA-EGFP using lipofectamine 2000 (ThermoFisher Scientific) according to the manufacturer's protocol. Cells were harvested 72 h post-transfection. 30 µg cell lysates was electrophoretically separated on a Mini-PROTEAN TGX Gel, 4–15% (Bio-Rad) and transferred to nitrocellulose membranes (LI-COR Bioscience) for 1 h. For quantification of loading control, total protein stain was performed using REVERT Total Protein Stain (LI-COR Bioscience, cat. no. 926-11010), following the manufacturer's instructions. Nitrocellulose membranes were blocked for > 60 min at room temperature with blocking buffer (Licor Odyssey Blocking Buffer) and then were probed overnight at 4 °C with primary antibodies against rabbit anti-TRIP8b antibody (from D.M.C.) and GAPDH (Millipore, cat. no. MAB374) in blocking buffer (LI-COR Odyssey Blocking Buffer). The following day, blots were rinsed and incubated in IRDye 680LT goat anti–mouse IgG (H + L; LI-COR Bioscience, cat. no. P/N 925-68020) and IRDye 800CW donkey anti–rabbit IgG (H + L; LI-COR Bioscience, cat. no. P/N 926-32213) in blocking buffer (Licor Odyssey Blocking Buffer). Immunoreactive bands were visualized using an Odyssey CLx chemifluorescence detector (LI-COR) with quantitation performed using LI-COR Image Studio 5.x. The signal intensity of TRIP8b was normalized to the signal intensity of each lane of total protein staining[60].

Tissue collection and immunohistochemistry. Mice were anesthetized with chloral hydrate (Sigma-Aldrich, cat. no. C8383, 400 mg/kg, stock solution 400 mg/ml made in 0.9% NaCl solution, i.p.) and underwent intracardial exsanguination with cold 0.1 M PBS (7 ml/min, 6 min) followed by perfusion with 4% paraformaldehyde in 0.1 M PBS (15 min). After subsequent cryoprotection, brains were sectioned coronally on a freezing microtome (Leica), and 30-µm sections through the entire A/P length of the hippocampus and entorhinal cortex (from bregma: –0.82 to –4.24 mm) were collected. Serial sets of sections were stored in 0.1% NaN_3 in 1 × PBS at 4 °C until processing for slide-mounted immunohistochemistry (IHC) analysis[36,61].

For Ki67, DCX, BrdU, GFP, TRIP8b, NeuN, and mCherry IHC, one series of sections was mounted on glass slides (Superfrost/Plus, Fisher) that were coded to ensure experimenters remained blind throughout quantification and analysis of data. Sections were processed for antigen retrieval (0.01 M citric acid, pH 6.0, 95 °C, 15 min), and nonspecific staining was blocked via incubation in blocking solution (3% normal donkey serum (NDS), vol/vol in 0.1% Triton X-100 in 1 × PBS) for 30 min. For BrdU IHC, permeabilization was performed using 0.1% Trypsin in 0.1 M Tris and 0.1% $CaCl_2$, and denaturation was performed using 2 N HCl in 1 × PBS before the blocking step. After blocking, sections were incubated with one of the following primary antibodies: rabbit anti-Ki67 (1:500; Thermo Scientific, cat. no. RM-9106), goat anti-DCX (1:500; Santa Cruz, cat. no. SC-8066), rat anti-BrdU (1:800; Accurate Chemicals cat. no. Obt0030), chicken anti-GFP (1:3,000; Aves cat. no. GFP-1020), guinea pig anti-TRIP8b (1:500; from D.M.C.), mouse anti-TRIP8b1a5 (1:500; from D.M.C.), rabbit anti-mCherry (1:1,000; Clontech, cat. no. 632496) in 0.1% Tween-20 in 1 × PBS overnight. For BrdU and NeuN double-labeling IHC, sections were incubated in mouse anti-NeuN (1:500; Millipore, cat no. MAB377, Billerica, MA) and rat anti-BrdU (1:800; Accurate Chemicals, cat. no. Obt0030). After incubation with primary antibody, sections for single-labeling IHC were rinsed and incubated in the appropriate secondary antibody: biotinylated donkey anti–rabbit IgG (cat. no. 711-065-162), biotinylated donkey anti–goat IgG antibody (cat. no. 705-065-003), biotinylated donkey anti–rat IgG (cat. no. 712-065-153), biotinylated donkey anti–chicken IgY (cat. no. 703-065-155), biotinylated donkey anti–guinea pig IgG (cat. no. 706-065-148) or biotinylated donkey anti–mouse IgG (cat. no. 715-065-150; all 1:200, Jackson ImmunoResearch Laboratories Inc., West Grove, PA) in 1.5% NDS in 1 × PBS for 1 h. After rinses and 30 min in 0.3% hydrogen peroxide in 1 × PBS, sections were incubated in avidin–biotin complex (ABC Elite, Vector Laboratories) for 60 min. After rinsing, staining was visualized using DAB/metal concentration (Thermo Scientific, cat. no. 1856090) or fluorescein-, cyanine-3-,or cyanine-5-labeled Tyramide Signal Amplification (TSA, PerkinElmer, cat. no. SAT701, no. SAT704 or no. SAT705, respectively). For BrdU and NeuN double-labeling IHC, after incubation with a NeuN-targeted primary antibody, sections were incubated in cyanine-5-labeled donkey anti-mouse secondary antibody (Jackson ImmunoResearch Laboratories Inc., cat. no. 715-175-150), fixed with 4% paraformaldehyde for 15 min and then incubated with anti-BrdU primary antibody. This was followed by incubation in biotinylated donkey anti-rat secondary antibody (Jackson ImmunoResearch Laboratories Inc., cat. no. 712-065-153) and then ABC Elite, and immunostaining was finally visualized via incubation in fluorescein–TSA (TSA, PerkinElmer, cat. no. SAT701). Nuclear Fast Red (Vector Laboratories, cat. no. H-3403), DAPI (Roche, cat. no. 236276) or Neurotrace 500/525 green fluorescent Nissl (Invitrogen, cat. no. N-21480) were used as counterstains.

Assessment and quantification of immunoreactive soma and terminals. Unbiased analysis of $Ki67^+$, $BrdU^+$, DCX^+, GFP^+, and c-Fos^+ cell numbers in the DG was performed via stereologic quantification on a BX51 System Microscope (Olympus America, Center Valley, PA, USA) by an observer blind to experimental condition as previously described[36,62]. $Ki67^+$ subgranular zone (SGZ) cells, $BrdU^+$ granule cell layer (GCL) cells, GFP^+ SGZ type-1 radial glial-like DG cells, and c-Fos^+ GCL cells were visualized with a 40×, 0.63 NA oil-immersion objective. Cell number was quantified with the formula: total population of cells = total cells counted × (1 / ssf) × (1 / asf) × (1 / hsf), where ssf is the section sampling fraction (Ki67: 1/9; BrdU, GFP, and c-Fos: 1/8), asf is the area sampling fraction (1 for the rare populations of $Ki67^+$, $BrdU^+$, GFP^+, and c-Fos^+ cells; thus, these cells were counted in 1 of every 9th section or 1 of every 8th section throughout the DG), and hsf is the height sampling fraction (1 given the minimal effect edge artifacts have in counting soma < 10 µm in diameter with ssf 1/9 or 1/8). As $Ki67^+$ cell number was counted in both hemispheres, the resulting formula was: total population of $Ki67^+$ cells = total cells counted × (1 / (1 / 9)) × (1 / 1) × (1 / 1). BrdU, GFP, and c-Fos were counted in one hemisphere, and thus the resulting formula was: total population of $BrdU^+$ cells, GFP^+ cells, or c-Fos^+ cells = (total cells counted × (1 / (1 / 8)) × (1 / 1) × (1 / 1)) × 2.

For bregma graphs of immunoreactive cells, the number of cells was examined per coronal section over the rostrocaudal axis of the DG, and the *x* axis displays the distance from bregma in mm. For qualitative assessment of TRIP8b protein expression in specific brain regions of wild-type mice and TRIP8b knockout mice (Supplementary Fig. 2i), relative TRIP8b protein expression in the parietal cortex, Ent, and hippocampal subregions was examined via epifluorescence under magnification (400×) and were ranked from – (not detected) to + + + (greatest relative expression). For assessment of GFP or mCherry protein expression in specific brain regions after infusion of virus in the Ent (Figs. 2–5 and Supplementary Figs. 2 and 4–11), stained sections were examined for the presence of GFP^+ or $mCherry^+$ soma or terminals via epifluorescence under magnification (400×).

For c-Fos^+ cell density in the Ent, cells were visualized with a 20× objective, and images of c-Fos^+ cells in lEnt and mEnt (two images per subject; $n = 5$ mCherry-infused mice and 4 hM3Dq-infused mice) were taken using a DP74 camera with Cellsens software (Olympus America, Center Valley, PA, USA) and cell number was quantified using ImageJ software with automated analysis (National Institutes of Health, Bethesda, Maryland, USA)[63]. Cross-sectional areas

of the lEnt and mEnt were measured using Cellsens standard software (ver. 1.16, Olympus America, Center Valley, PA, USA).

For the DCX$^+$ population of GCL cells, which were not rare, cells were visualized with a 0.75 NA (DCX) oil-immersion objective. The Optical Fractionator Probe within Stereo Investigator software (ver. 11.03, MBF Bioscience, Williston, VT, USA) was then applied, and an unbiased counting frame was superimposed on the region of interest using a MicroFIRE A/R camera (Optronics, Goleta, CA, USA). To account for tissue shrinkage, an optical dissector height of 12 µm was applied. The number of DCX$^+$ cells in tissue from *Trip8b* knockout and control mice was counted in both hemispheres, and the number of DCX$^+$ cells in tissue from TRIP8b-shRNA-infused and SCR-shRNA-infused mice were counted in one hemisphere. As the ssf was 1/9 (*Trip8b* knockout mice studies) or 1/8 (TRIP8b shRNA studies), total counts were multiplied by 9 or 16 to obtain the total number of DCX$^+$ GCL or DG cells.

Confocal microscopy and colocalization analyses. Colocalization of immunoreactive cells was assessed by an observer blinded to experimental condition using confocal microscopy (LSM510-META, Carl Zeiss, Oberkochen, Germany; emission wavelengths were 488 nm and 633 nm)[64]. Analyses were performed using a 63×, 1.2-NA water-immersion lens. 50–100 BrdU$^+$ cells were analyzed in five or six brain sections from the anterior, middle, and posterior hippocampal GCL of each mouse and were classified as NeuN$^+$ or NeuN$^-$ through analysis of adjacent Z-sections, orthogonal sectioning through Z-sections, and 3D reconstruction with rotation. The percent of BrdU$^+$ cells that were also NeuN$^+$ in each mouse was multiplied by the total number of BrdU$^+$ cells for each mouse, which was obtained via stereology. The resulting numbers of BrdU$^+$NeuN$^+$ cells for each mouse were combined for each group and subjected to statistical analysis.

Dendritic tree reconstruction. Dendrite and cell body morphological analyses of DCX$^+$ neurons stained with DAB were performed by an observer blind to experimental condition using NeuroLucida software (ver. 10, MBF Bioscience) on a BX51 System Microscope (Olympus America, Center Valley, PA, USA) and a 40×, 0.75-NA oil-immersion lens with a MicroFIRE A/R camera (Optronics, Goleta, CA, USA). DCX$^+$ cells selected for tracing had three or more nodes, and the cell body and branches were visible within the thickness of the section. The dendritic tree and cell body of each cell was traced in its entirety with an unbiased systematic random sampling of the visual field[20]. 6–8 DCX$^+$ neurons from anterior (−1.46 to −2.06 mm from bregma) and posterior (−2.76 to −3.28 mm from bregma) DG sections that were spaced equally throughout the A/P axis of the hippocampus were analyzed. The coordinate files generated through 3D reconstruction were analyzed in NeuroLucida Explorer, generating morphologic measurements for each neuron that included cell body cross section, dendrite length and surface area, number of nodes and endings, and maximum branch order.

Behavioral tests. Brief descriptions of the behavioral tests are provided below. Male or female mice were used for behavioral tests, as described below, and behavior tests were done during the light cycle unless otherwise noted. Behavioral scoring was done by a single rater, blind to the treatment condition.

Chronic social defeat stress and social interaction test. Exposure to social defeat and subsequent interaction testing was performed as described previously[18,25,36]. Retired male CD1 breeders (4–6 months old; Charles River Laboratories, Wilmington, MA) were screened for aggressiveness. If a CD1 mouse took <60 s to attack a test mouse (C57BL/6J mouse) placed into the home cage and displayed this latency to attack for two consecutive days, the CD1 mouse was determined to be aggressive. For CSDS, a CD1 aggressor mouse was housed on one side of a cage, which was partitioned with a plastic divider, and a test mouse (C57BL/6J or CamKIIα-iCre) was placed on the other side of the divider. Two to three hours before the onset of the dark cycle, the 'defeat' bout was triggered by removing the plastic divider for 5 (C57BL/6J experiments) or 10 (CamKIIα-iCre experiments) min, which allowed the CD1 aggressor to physically attack the test mouse. The test mouse was moved to a different cage opposite a new aggressor either after the defeat bout (C57BL/6J experiments) or immediately before the next defeat (CamKIIα-iCre experiments) in order to instill generalization of stress-induced defeat to the CD1 strain, not to just a single aggressor. Control mice were housed in partitioned cages identical to those used for defeat, but they were housed opposite to one other control mouse. Control mice were handled each day at the same time of day as when the defeat was performed. The defeats or handling continued daily for 10 d.

On day 11 (24 h after the last day of the 10-d CSDS), social interaction was measured via two trials lasting 150 s each. Test mice were individually placed in the new environment of a white open-field chamber (length, 45 cm × width, 45 cm × height, 30 cm) with a discrete 'interaction zone' against one wall (length, 14 cm × width, 26 cm) that encompassed an empty plastic enclosure (length, 6.5 cm × width, 10 cm × height, 42 cm; Nationwide Plastics custom order). For the first trial (2 min 30 s in duration), the mouse was placed randomly into either corner opposite to the interaction zone, and the movements of the mouse were tracked using Ethovision software (Noldus Information Technology). Specifically, the time the mouse spent in the interaction zone or corners opposite to the interaction zone was quantified. For the second trial, which was also 2 min 30 s in duration and which began ~30 s after the first trial was completed, an unfamiliar CD1 aggressor mouse was placed into the plastic enclosure in the interaction zone. The SI ratio was calculated as follows: SI = (time spent in interaction zone with aggressor mouse) / (time spent in interaction zone with empty enclosure present). Mice with a SI ratio <1 were categorized as susceptible, and mice with a SI ratio ≥ 1 were categorized as resilient. The distribution of SI ratios is shown in Supplementary Fig. 3f, and the weights of the mice on Day 1 and 11 of CSDS is shown in Supplementary Fig. 3g. Immediately after testing for SI, mice were singly housed until they were euthanized 24 h later.

Locomotor test. Mice were individually placed in a cage with fresh bedding, and the cage was placed between photocells under dim or red lights during the light cycle and under red lights during the dark cycle. A computer-controlled photobeam activity system (San Diego Instruments) recorded the total movement of mice in the *XY* plane; photocell beam breaks were recorded in 5-min bins for 17 or 20 h. In Fig. 3i, one mouse from the TRIP8b/IRR group was excluded due to a husbandry error (the water bottle flooded the cage during the locomotor test).

Restraint stress. Except for under the basal condition (Fig. 3a–e) or under conditions that modeled stress (CORT, Fig. 4a–g; CSDS experiments, Fig. 5s–t), mice were restrained for 30 min before depressive-like behavior tests (i.e., forced swim test and novelty-suppressed feeding test)[24]. The restraint apparatus (50-ml falcon tube) restricted movement but did not interfere with normal breathing, as it was modified with numerous holes.

Forced swim test. The forced swim test was performed to evaluate behavioral despair induced by stress, as previously described[65,66]. Mice were placed in a 5-L beaker (Corning Inc. Life Sciences, Lowell, MA, USA) that was filled with 4 L of 25 ± 2 °C water, and the entire session was videotaped. For the last 4 min (Fig. 3c) or the total 6 min (Figs. 3j and 4g and Supplementary Figs. 5i–k, 7b, and 8b) of the session, the latency to immobility and time spent immobile (or the normalized total immobile time) were measured.

Novelty-suppressed feeding test. Group-housed mice were food-deprived for 18 h. For the novelty-suppressed feeding test, a single pellet of regular mouse food chow was placed in the center of a new open-field arena (length, 44 cm × width, 44 cm × height, 30 cm) under dim light[24,35]. A mouse was placed in a corner of the arena and allowed to explore for up to 12 min. The trial ended when the mouse initially bit and consumed the chow. After the NSF test, the mouse was immediately removed from the test arena and placed individually in the home cage where it was presented with a preweighed amount of chow for 5 min. The food was weighed at the end of the session, and the amount consumed (difference) was recorded in grams.

Contextual fear conditioning test and cue fear conditioning test. Context- and cue-dependent fear conditioning experiments were performed using a contextual conditioning system (Med Associates, St. Albans, VT, USA) as previously described[64]. Mice were trained and tested in the contextual and cued fear conditions within the chamber (length, 25 cm × width, 29 cm × height, 25 cm) with clear plastic walls and ceilings and a standard floor made of metal bars. For training, after 2-min habituation, a tone was presented (80 dB white noise, 30 s), which co-terminated with a footshock (0.5 mA, 2 s). The tone–shock pairing was repeated for a total of three shocks over 6 min with a 1-min interval between tone presentations. For the contextual conditioning test, 24 h after training, mice were placed into the training context for 5 min, but the tone and shock were not presented. For the cued conditioning test, 48 h after training, mice were placed in a new environment (plastic floor over the grid bars, triangle roof, vanilla scent) for 6 min, with the tone presented continuously for the last 3 min. Scoring of freezing behavior was automatically performed by the Med Associates software using a threshold of 20 arbitrary units and minimum freeze duration of 0.5 s.

Dark–light test. The apparatus consisted of a polypropylene cage (length, 44 cm × width, 21 cm × height, 21 cm) unequally divided into two chambers (two-thirds and one-third of the space) by a wall with a small vestibule. The large chamber was open, transparent, and brightly illuminated by two 20-W fluorescent lights (measured as 1,388 lux at cage floor), and the small chamber was closed, painted black, and dark. Initially, the mouse was placed in the dark side for 2 min, and the transitions of the mouse between the two chambers were automatically detected via four photocells located in the vestibule over 10 min. The time spent in the brightly lit side and the latency to enter the brightly lit side were measured by the automated system.

Elevated plus maze. The apparatus was built (elevation, 99 cm; two open and two closed arms, each length, 67 cm × width, 6 cm; closed arm walls, height, 17 cm) as previously described[67]. Mice were placed in the center of the apparatus and allowed to freely explore for 5 min under dim light. The time spent in open or closed arms and the frequency in each arm were scored via Ethovision software (Noldus Information Technology).

Splash test. Mice were singly housed a day before the test. The day of the test, the nestlet was removed from their home cage at least 1 h before the test, as previously

described[68]. A freshly made 10% sucrose solution was placed into a fine water spray mister, and the nozzle was depressed a single time to dispense solution onto the back (dorsal) region. Grooming activity (frequency and duration) was recorded for 5 min after the application of the solution.

Image presentation. For image presentation, journal guidelines were applied (www.nature.com/authors/policies/image.html/). For western blot analyses, images of adjacent immunoreactive bands were captured using 3CCD color video camera (Sony, cat. no. DCX-3900), and intensities were analyzed through densitometry using Scion image software (Scion Corporation). Full western blot images are provided in Supplementary Fig. 3 and Supplementary Fig. 4. Photomicrographs of immunostained tissue sections were collected on either a DP74 camera with Cellsens software (Olympus America, Center Valley, PA, USA) or a MicroFIRE A/R camera (Optronics, Goleta, CA, USA). Orthogonal images were captured using confocal microscopy (LSM510-META, Carl Zeiss, Oberkochen, Germany; emission wavelengths 488 nm and 633 nm)[64], and analyses were performed using a 63×, 1.2-NA water-immersion lens through analysis of adjacent Z-sections, orthogonal sectioning through Z-sections, and 3D reconstruction with rotation. Scale bar photomicrographs were collected at the time of image collection. After collection of images, files were opened in Adobe Photoshop, and images were cropped. Equal adjustments (brightness, contrast) in the control and experimental group were made to the entire image; only linear adjustments were made[69]. Where red and green images were both present in a single image, images were color-shifted in Photoshop to enable visualization by color-blind individuals[69]. Processed images were then opened in Adobe Illustrator, panel indicators (arrowheads, dotted lines, molecular weight indicators) were added, and final figures were assembled.

Statistical analysis. Data are reported as mean ± s.e.m. Prior to statistical analyses, data assumptions (for example, normal distribution, similar variation between experimental groups, etc.) were verified. Statistical approaches and results are provided in Supplementary Table 1, statistical analysis summaries are provided in the figure legends, and additional information can be found in the Life Sciences Reporting Summary that accompanies this paper and is available online. Analyses with two groups were performed using an unpaired, two-tailed Student's *t*-test, and significance is indicated by asterisks in this case (e.g., $^{*}P<0.05$, $^{**}P<0.01$, $^{***}P<0.001$). Analyses with more than two groups and one variable were performed using one-way ANOVA and either Bonferroni post hoc test or Fisher's LSD post hoc test; post hoc significance is indicated by asterisks in this case (e.g., $^{*}P<0.05$, $^{**}P<0.01$, $^{***}P<0.001$). Analyses with more than two variables were performed using two-way ANOVA with Bonferroni post hoc test or Fisher's LSD post hoc test; post hoc significance is indicated by lowercase letters in this case (e.g., *a*, $P<0.05$; *a′*, $P<0.01$; *a″*, $P<0.001$). Repeated measures (RM) were used where appropriate, as indicated in the figure legends and in Supplementary Table 1. For the correlation between DG TRIP8b isoform levels and the SI ratio, a linear regression was performed, and the r^2 and *P* values were reported. Statistics were performed using GraphPad Prism software (ver. 6.0, ver. 7.0). Statistical significance was defined as $P<0.05$, and exact *P* values and *F* values are provided in Supplementary Table 1. For all molecular and behavioral studies, mice were randomly assigned to groups. Many behavioral and cellular results were confirmed via independent replication of the experiments, as shown in Supplementary Table 1. Additionally, investigators were blinded to the treatment group until all data had been collected. Most behavioral and cellular results were confirmed via at least one independent replication (i.e., Figs. 1, 2h,j,n–w, 3i,j, 4b–g, and 5g–t and Supplementary Figs. 1b–m, 3a–l, 4a–e, 5i–k, 7a,b, 8a,b, 9a–f, and 11e–g). Sample sizes were determined on the basis of extensive laboratory experience and were verified via power analysis.

Reporting Summary. Further information on experimental design is available in the Nature Research Reporting Summary linked to this article.

Code availability. MatLab code for spike and frequency analysis of in vivo EEG experiments can be accessed via contacting R.C.A.N. at ahrensnicklasr@email.chop.edu.

Data availability. The data sets generated during and/or analyzed during the current study are available from the corresponding author on reasonable request.

References

51. Yamaguchi, M., Saito, H., Suzuki, M. & Mori, K. Visualization of neurogenesis in the central nervous system using nestin promoter-GFP transgenic mice. *Neuroreport* **11**, 1991–1996 (2000).
52. Hommel, J. D., Sears, R. M., Georgescu, D., Simmons, D. L. & DiLeone, R. J. Local gene knockdown in the brain using viral-mediated RNA interference. *Nat. Med.* **9**, 1539–1544 (2003).
53. Zolotukhin, S. et al. Recombinant adeno-associated virus purification using novel methods improves infectious titer and yield. *Gene Ther.* **6**, 973–985 (1999).
54. Mandyam, C. D., Harburg, G. C. & Eisch, A. J. Determination of key aspects of precursor cell proliferation, cell cycle length and kinetics in the adult mouse subgranular zone. *Neuroscience* **146**, 108–122 (2007).
55. Alonso, A. & Klink, R. Differential electroresponsiveness of stellate and pyramidal-like cells of medial entorhinal cortex layer II. *J. Neurophysiol.* **70**, 128–143 (1993).
56. Corbett, B. F. et al. Sodium channel cleavage is associated with aberrant neuronal activity and cognitive deficits in a mouse model of Alzheimer's disease. *J. Neurosci.* **33**, 7020–7026 (2013).
57. Dengler, C. G., Yue, C., Takano, H. & Coulter, D. A. Massively augmented hippocampal dentate granule cell activation accompanies epilepsy development. *Sci. Rep.* **7**, 42090 (2017).
58. Clarkson, R. et al. Characterization of image quality and image-guidance performance of a preclinical microirradiator. *Med. Phys.* **38**, 845–856 (2011).
59. Spencer, S. et al. Circadian genes Period 1 and Period 2 in the nucleus accumbens regulate anxiety-related behavior. *Eur. J. Neurosci.* **37**, 242–250 (2013).
60. Eaton, S. L. et al. Total protein analysis as a reliable loading control for quantitative fluorescent Western blotting. *PLoS One* **8**, e72457 (2013).
61. Ables, J. L. et al. Notch1 is required for maintenance of the reservoir of adult hippocampal stem cells. *J. Neurosci.* **30**, 10484–10492 (2010).
62. DeCarolis, N. A. et al. In vivo contribution of nestin- and GLAST-lineage cells to adult hippocampal neurogenesis. *Hippocampus* **23**, 708–719 (2013).
63. Schneider, C. A., Rasband, W. S. & Eliceiri, K. W. NIH Image to ImageJ: 25 years of image analysis. *Nat. Methods* **9**, 671–675 (2012).
64. Petrik, D. et al. Functional and mechanistic exploration of an adult neurogenesis-promoting small molecule. *FASEB J.* **26**, 3148–3162 (2012).
65. Krishnan, V. & Nestler, E. J. The molecular neurobiology of depression. *Nature* **455**, 894–902 (2008).
66. Nakasato, A. et al. Swim stress exaggerates the hyperactive mesocortical dopamine system in a rodent model of autism. *Brain Res.* **1193**, 128–135 (2008).
67. Mulder, G. B. & Pritchett, K. The elevated plus-maze. *Contemp. Top. Lab. Anim. Sci.* **43**, 39–40 (2004).
68. Surget, A. et al. Drug-dependent requirement of hippocampal neurogenesis in a model of depression and of antidepressant reversal. *Biol. Psychiatry* **64**, 293–301 (2008).
69. Johnson, J. Not seeing is not believing: improving the visibility of your fluorescence images. *Mol. Biol. Cell* **23**, 754–757 (2012).